



<b>Publication Year</b>	2022
<b>Acceptance in OA @INAF</b>	2023-05-22T09:18:53Z
<b>Title</b>	IBIS-A: The IBIS data Archive. High resolution observations of the solar photosphere and chromosphere with contextual data
<b>Authors</b>	ERMOLLI, Ilaria; GIORGI, Fabrizio; MURABITO, Mariarita; Marco Stangalini; Vincenzo Guido; et al.
<b>DOI</b>	10.1051/0004-6361/202142973
<b>Handle</b>	<a href="http://hdl.handle.net/20.500.12386/34166">http://hdl.handle.net/20.500.12386/34166</a>
<b>Journal</b>	ASTRONOMY & ASTROPHYSICS
<b>Number</b>	661

# IBIS-A: The IBIS data Archive

## High-resolution observations of the solar photosphere and chromosphere with contextual data<sup>★</sup>

Ilaria Ermolli<sup>1</sup>, Fabrizio Giorgi<sup>1</sup>, Mariarita Murabito<sup>1</sup>, Marco Stangalini<sup>2,1</sup>, Vincenzo Guido<sup>1</sup>, Marco Molinaro<sup>3</sup>, Paolo Romano<sup>4</sup>, Salvatore L. Guglielmino<sup>4</sup>, Giorgio Viavattene<sup>1</sup>, Gianna Cauzzi<sup>5,6</sup>, Serena Criscuoli<sup>6</sup>, Kevin P. Reardon<sup>6</sup>, and Alexandra Tritschler<sup>6</sup>

<sup>1</sup> INAF–Osservatorio Astronomico di Roma, via Frascati 33, 00078 Monte Porzio Catone, Italy  
e-mail: [ilaria.ermolli@inaf.it](mailto:ilaria.ermolli@inaf.it)

<sup>2</sup> ASI Agenzia Spaziale Italiana, via della Ricerca Scientifica, Roma, Italy

<sup>3</sup> INAF–Osservatorio Astronomico di Trieste, Via Giambattista Tiepolo, 11, 34131 Trieste, Italy

<sup>4</sup> INAF–Osservatorio Astrofisico di Catania, Via S. Sofia 78, 95123 Catania, Italy

<sup>5</sup> INAF–Osservatorio Astrofisico di Arcetri, Largo Enrico Fermi 5, 50125 Firenze, Italy

<sup>6</sup> National Solar Observatory, 3665 Discovery Drive, Boulder CO 80303, USA

Received 21 December 2021 / Accepted 4 February 2022

### ABSTRACT

**Context.** The IBIS data Archive (IBIS-A) stores data acquired with the Interferometric BIdimensional Spectropolarimeter (IBIS), which was operated at the Dunn Solar Telescope of the US National Solar Observatory from June 2003 to June 2019. The instrument provided series of high-resolution narrowband spectropolarimetric imaging observations of the photosphere and chromosphere in the range 5800–8600 Å and co-temporal broadband observations in the same spectral range and with the same field of view as for the polarimetric data.

**Aims.** We present the data currently stored in IBIS-A, as well as the interface utilized to explore such data and facilitate its scientific exploitation. To this end, we also describe the use of IBIS-A data in recent and undergoing studies relevant to solar physics and space weather research.

**Methods.** IBIS-A includes raw and calibrated observations, as well as science-ready data. The latter comprise maps of the circular, linear, and net circular polarization, and of the magnetic and velocity fields derived for a significant fraction of the series available in the archive. IBIS-A furthermore contains links to observations complementary to the IBIS data, such as co-temporal high-resolution observations of the solar atmosphere available from the instruments onboard the Hinode and IRIS satellites, and full-disk multi-band images from INAF solar telescopes.

**Results.** IBIS-A currently consists of 30 TB of data taken with IBIS during 28 observing campaigns performed in 2008 and from 2012 to 2019 on 159 days. Of the observations, 29% are released as Level 1 data calibrated for instrumental response and compensated for residual seeing degradation, while 10% of the calibrated data are also available as Level 1.5 format as multi-dimensional arrays of circular, linear, and net circular polarization maps, and line-of-sight velocity patterns; 81% of the photospheric calibrated series present Level 2 data with the view of the magnetic and velocity fields of the targets, as derived from data inversion with the Very Fast Inversion of the Stokes Vector code. Metadata and movies of each calibrated and science-ready series are also available to help users evaluate observing conditions.

**Conclusions.** IBIS-A represents a unique resource for investigating the plasma processes in the solar atmosphere and the solar origin of space weather events. The archive currently contains 454 different series of observations. A recently undertaken effort to preserve IBIS observations is expected to lead in the future to an increase in the raw measurements and the fraction of processed data available in IBIS-A.

**Key words.** Sun: atmosphere – Sun: photosphere – Sun: chromosphere – methods: data analysis – astronomical databases: miscellaneous

## 1. Introduction

The solar atmosphere is a highly structured, complex, and strongly dynamic environment produced by the continuous interplay between unmagnetized and magnetized plasmas that permeate it (e.g., Rempel & Schlichenmaier 2011; Stein 2012; Cheung & Isobe 2014; van Driel-Gesztelyi & Green 2015; Bellot Rubio & Orozco Suárez 2019; Wiegmann & Sakurai 2021). This

interplay drives the Sun's activity and radiative variability on timescales from seconds to centuries. In addition, it imposes electromagnetic forces in the whole heliosphere by modulating the solar particulate and magnetic flux (e.g., Kilpua et al. 2017; Temmer 2021). The same interplay also plays a fundamental role in hugely diverse astrophysical systems. For example, in addition to being responsible for the evolution of magnetic features, coronal heating, and wind acceleration in the solar and stellar atmospheres (e.g., Schmelz 2003), it is responsible for the acceleration of jets from active galactic nuclei and gamma

<sup>★</sup> Research supported by the H2020 SOLARNET grant no. 824135.

ray bursts (e.g., [Blandford et al. 2019](#)) and for the heating of the warm-ionized medium of galaxies (e.g., [Padoan & Nordlund 2011](#)). In all these systems unmagnetized and magnetized plasmas interrelate on small spatial and temporal scales that are still beyond those achievable with current telescopes. However, these scales will be accessible soon in the Sun's atmosphere with the upcoming 4 m class solar telescopes such as the National Science Foundation's *Daniel K. Inouye* Solar Telescope (DKIST, [Rimmele et al. 2020](#); [Rast et al. 2021](#)) and the European Solar Telescope (EST, [Collados et al. 2013](#); [Schlichenmaier et al. 2019](#)).

Nevertheless, analysis of high-resolution multi-wavelength spectropolarimetric observations of the Sun's atmosphere performed over the past two decades have already yielded a wealth of information on the interaction between unmagnetized and magnetized plasmas (e.g., [van Driel-Gesztelyi & Green 2015](#); [Jess et al. 2015](#); [Borrero et al. 2017](#); [Bellot Rubio & Orozco Suárez 2019](#)). These observations include data acquired with the Interferometric BiDimensional Spectrometer (IBIS, [Cavallini 2006](#)), which combined dual tunable Fabry-Perot interferometers with a high-order adaptive optics system and short exposures, to perform high-resolution solar studies.

IBIS was developed at the INAF Arcetri Astrophysical Observatory with contributions from the Universities of Florence and Rome Tor Vergata. It was installed at the Dunn Solar Telescope (DST) of the National Solar Observatory (NSO) in New Mexico (USA) in June 2003, on an optical bench fed by a high-order adaptive optics system. It was operated there by INAF and NSO from 2005 to 2019 as a facility instrument. In 2019 the instrument was dismantled for refurbishing in light of its reinstallation at a different telescope ([Ermolli et al. 2020](#)).

From 2003 to 2019 IBIS provided data of the solar photosphere and chromosphere at high spectral, spatial, and temporal resolution over a relatively large field of view (FOV); more details are presented in Sect. 2.2. These data were often acquired simultaneously to those from other instruments installed at the DST, for example the Rapid Oscillations in the Solar Atmosphere (ROSA, [Jess et al. 2010](#)) and the Facility Infrared Spectrometer (FIRS, [Jaeggli et al. 2012](#)). In addition, IBIS often observed co-temporally with other instruments in the framework of coordinated observing campaigns with space-borne telescopes, for example the Solar and Heliospheric Observatory/Michelson Doppler Imager (SOHO/MDI, [Scherrer et al. 1995](#)), Hinode/Solar Optical Telescope (Hinode/SOT, [Tsuneta et al. 2008](#)), Solar Dynamics Observatory/Heliographic and Magnetic Imager (SDO/HMI, [Scherrer et al. 2012](#)), SDO/Atmospheric Imaging Assembly (SDO/AIA, [Lemen et al. 2012](#)), Interface Region Imaging Spectrograph (IRIS, [De Pontieu et al. 2014](#)), and ground-based telescopes, such as the New Solar Telescope (NST, [Cao et al. 2010](#)) and Atacama Large Millimeter/submillimeter Array (ALMA, [Wedemeyer et al. 2020](#)). With the DST located in the mountains above the White Sands Missile Range, IBIS also co-observed with many solar sounding rocket payloads launched from the range, including the Extreme Ultraviolet Normal Incidence Spectrograph (EUNIS, [Brosius et al. 2014](#)), High Resolution Coronal Imager (Hi-C, [Kobayashi et al. 2014](#)), Chromospheric Lyman-Alpha Spectro-Polarimeter (CLASP, [Narukage et al. 2016](#)), and Very high Angular resolution Ultraviolet Telescope (VAULT, [Vourlidas et al. 2016](#)). Instead, due to different time zones and telescope operations, there are few if any contemporary observations between IBIS and other spectropolarimetric instruments installed at the solar telescopes on the Canary Islands, for example the CRisp Imaging Spectro-Polarimeter (CRISP, [Scharmer et al. 2008](#)) and the CHROMospheric

Imaging Spectrometer (CHROMIS, [Scharmer et al. 2019](#)) operating at the Swedish 1-m Solar Telescope (SST, [Scharmer et al. 2003](#)).

Given the versatility of the instrument, IBIS data have been used to study a variety of topics, including the temporal evolution and 3D nature of plasma flow in quiet regions ([Del Moro et al. 2007](#)) and large-scale magnetic features ([Giordano et al. 2008](#); [Sobotka et al. 2012, 2013](#)); turbulent solar convection ([Viavattene et al. 2020, 2021](#)); structure and brightness of small- ([Viticchié et al. 2009, 2010](#); [Romano et al. 2012](#)) and large-scale magnetic features ([Criscuoli et al. 2012](#)); dissipation of magnetic energy by current sheets above sunspot umbrae ([Tritschler et al. 2008](#)); identification, formation, and decay of active regions ([Ermolli et al. 2017](#); [Zuccarello et al. 2009](#); [Murabito et al. 2016, 2017](#); [Schilliro & Romano 2021](#)); formation, atmospheric stratification, and brightening in penumbral regions ([Romano et al. 2013, 2014, 2020](#); [Murabito et al. 2019, 2020a](#)); acoustic oscillations and MHD wave propagation in the solar atmosphere ([Vecchio et al. 2007, 2009](#); [Stangalini et al. 2011, 2012, 2013](#); [Sobotka et al. 2016](#); [Abbasvand et al. 2020](#); [Houston et al. 2020](#)) and in sunspots ([Stangalini et al. 2018, 2021a,b,c, 2022](#)); First Ionization Potential (FIP) effect ([Baker et al. 2021](#)); magnetic flux emergence from the photosphere to the chromosphere ([Murabito et al. 2020a](#)); chromospheric vortices ([Murabito et al. 2020b](#)); flares ([Kowalski et al. 2015](#); [Capparelli et al. 2017](#); [Romano et al. 2017](#)); sensitivity of spectral line diagnostics to temperature variations and small-scale magnetic fields ([Criscuoli et al. 2013](#)); and new spectroscopic diagnostics of the solar chromosphere ([Cauzzi et al. 2008, 2009](#); [Straus et al. 2008](#); [Reardon et al. 2009](#); [Judge et al. 2010](#); [Lipartito et al. 2014](#); [Molnar et al. 2019](#)).

Recently, an effort has been undertaken to collect the data acquired by the IBIS instrument and to preserve them in the permanent IBIS-Archive (IBIS-A). In this paper we describe the public release of the data available in IBIS-A. We introduce the IBIS observations and their processing in Sect. 2. We present the data available in IBIS-A and their quality in Sect. 3. We give an outline of the data access and examples of unexplored data available in IBIS-A in Sects. 4 and 5, respectively. Finally, we summarize this work and draw our conclusions in Sect. 6.

## 2. Observations and data processing

### 2.1. IBIS

The IBIS instrument ([Cavallini 2006](#)) basically consisted of two tunable Fabry-Pérot interferometers (FPs) and narrowband interference filters (hereafter pre-filters) operating in a classical mount over the spectral range 5800–8600 Å (later extended to 5400–8600 Å). During operations, the combination of the FPs, pre-filters, and instrument control allowed tuning the instrument transmission in wavelength sequentially through spectral lines isolated by the pre-filters. The number of wavelength points sampled per line, as well as the number of lines used in sequence, were defined by the observer depending on science target and available pre-filters.

It is worth noting that the layout and optical components of the IBIS instrument underwent improvements over time. For example, the addition of a polarimetric unit in 2006 expanded measurements at the spectral positions sampled by the instrument to all the Stokes polarization states (I, Q, U, V). After this upgrade, the instrument also underwent the implementation of new detectors and control software in 2010. However, these changes did not affect the main characteristics of the instrument

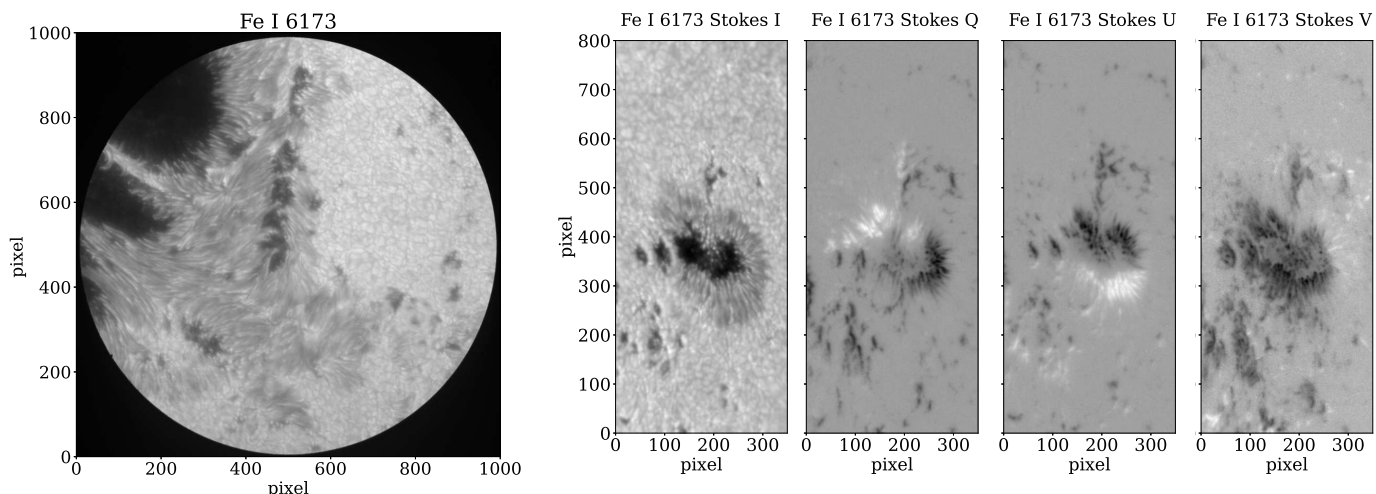


**Fig. 1.** Examples of IBIS data acquired (*from left to right*) in standard spectroscopic and spectropolarimetric modes at the Fe I 6173 Å line with circular ( $1000 \times 1000$  pixels<sup>2</sup>) and rectangular ( $350 \times 800$  pixels<sup>2</sup>) FOV on 25 October 2014, 15:32 UT and 13 May 2016, 13:38 UT at disk positions  $\mu = 0.85$  and  $\mu = 0.68$ , respectively. The spectroscopic and spectropolarimetric Stokes I observations were taken in the line continuum, while the spectropolarimetric Stokes Q and Stokes U and V data were acquired in the line core and line blue wing, respectively. Shown here are the Level 1 data derived from the instrumental calibrations and MOMFBD restoration (see Sects. 2.2 and 3.1 for more details).

described above. Moreover, from 2011 to 2019 the instrument had a rather stable condition with only minor modifications that did not significantly change the main characteristics of the data acquired by the instrument.

A thorough evaluation of the optical performance of IBIS is provided by Reardon & Cavallini (2008) and Righini et al. (2010). In brief, the instrument had a transmission profile with a full width at half maximum (FWHM) of 24.0 mÅ at 6328 Å (Reardon & Cavallini 2008) and a pixel scale of 0.082 arcsec per pixel (until 2010) or 0.098 arcsec per pixel (after 2010). These values allowed observations at the diffraction limit of the DST ( $\approx 0.16$  arcsec at 5800 Å). Further details concerning the IBIS data are found in Sect. 2.2.

## 2.2. Observing campaigns

A typical IBIS dataset consists of measurements taken in sequence over multiple spectral lines (two or three lines, e.g., Fe I at 6302 Å, Fe I at 6173 Å, and Ca II at 8542 Å), with each line sampled at several spectral positions (often between 10 and 30 positions), each position at six polarimetric modulation states ( $I \pm [Q, U, V]$ ), and each state with either a single exposure or multiple exposures. The data are characterized by a high spectral ( $R > 200\,000$ ), spatial ( $\approx 0.16$ – $0.24$  arcsec), and temporal (8–15 frames per second) resolution over a relatively large FOV (minimum linear dimension  $> 40$  arcsec; see details in the following). IBIS ensured a high wavelength stability in time of the instrumental profile (with a drift on the order of  $10 \text{ m s}^{-1}$  over 10 h), short exposure times to partially freeze the Earth’s atmospheric seeing (tens of ms), and nearly diffraction-limited resolution over the whole FOV.

The instrument could be operated in both the spectroscopic and spectropolarimetric modes. It also allowed for a hybrid mode where full-Stokes measurements were taken in some of the selected spectral lines while only spectral Stokes-I measurements were acquired for other lines. In standard spectroscopic mode the FOV was often circular with a diameter of  $\approx 95$  arcsec, as defined by a circular mask inserted in the entrance focal plane of the instrument. In standard spectropolarimetric mode the FOV

was rectangular with a dimension of  $\approx 40 \times 95$  arcsec<sup>2</sup>, as a result of the rectangular mask inserted in the focal entrance plane of the instrument so that the two orthogonally linear polarized beams could be imaged onto the same detector.

The spectroscopic and spectropolarimetric observational modes were both operated with acquisition of broadband (BB) images simultaneous to the narrowband (NB) data produced by the two FPs. The BB images allow for post-facto compensation of residual seeing degradation with enhancement of the image quality (Löfdahl 2016).

Figure 1 shows examples of IBIS data acquired in the standard spectroscopic and spectropolarimetric observational modes after instrumental calibrations and further processing described in Sect. 2.3. In particular, we show the spectroscopic observation at the photospheric Fe I 6173 Å line of a large sunspot region with umbral and penumbral areas imaged near the disk center, and the Stokes-I, -Q, -U, and -V measurements of a smaller sunspot region observed closer to the limb.

## 2.3. Data processing

IBIS-A includes the camera data originally generated by the instrument, as well as processed data. The latter were obtained with a reduction package built on the IBIS calibration pipeline (Criscuoli & Tritschler 2014) released by NSO<sup>1</sup> and with other codes. The NSO pipeline includes calibration for the dark current, for the flat-field response, and for the gain of the detectors; computation of the detector image scale and orientation; compensation for the artificial polarization introduced by the instrumentation and by the telescope; and calibrations for the systematic wavelength shift across the FOV due to the collimated mounting of the FPs and for residual effects of the seeing. In addition, the data available in IBIS-A were calibrated for pre-filter transmission curves and residual polarization cross-talk between Stokes-I and Stokes-Q, -U, -V data. Moreover, the BB data were processed for image restoration by using the

<sup>1</sup> <https://nso.edu/telescopes/dunn-solar-telescope/dst-pipelines/>

outcomes of the Multi-Object Multi-Frame Blind Deconvolution (MOMFBD, Löfdahl 2012; van Noort et al. 2005) in order to enhance the image quality over the full FOV. The package employed to process the data is written in IDL<sup>2</sup>, and it is run under a Linux Ubuntu distribution. The codes are run in semi-automatic mode, which requires inputs from the user at two steps in order to select the FOV for alignment of NB and BB images and to compute the residual polarization cross-talk. At present the MOMFBD restoration, which is written in C++, is not integrated in the data reduction package.

The IBIS measurements processed for the above steps form the Level 1 data in IBIS-A. At present there are 133 calibrated series out of the 454 series of raw IBIS observations stored in the archive.

A subset of the Level 1 observations was further processed to generate Level 1.5 data. This subset consists of the calibrated spectropolarimetric observations acquired at the photospheric Fe I 6173 Å and chromospheric Ca II 8542 Å lines under homogeneous instrumental setup (i.e., the same observing mode and spectral sampling).

The Level 1.5 data comprise maps of the mean circular polarization (CP), mean linear polarization (LP), and net circular polarization (NCP), and of the line-of-sight (los) velocity field ( $V_{\text{los}}$ ). The mean CP signal was estimated via two methods. The first involved computing the maximum amplitude of the Stokes-V spectral profile, as reported in Stangalini et al. (2021a), with the formula

$$\text{CP1} = \frac{|V_{\text{max}}|}{I_{\text{cont}}} \cdot \text{sign}(V_{\text{max}}), \quad (1)$$

where  $V_{\text{max}}$  is the maximum amplitude of the Stokes-V parameter in the measured profile and  $I_{\text{cont}}$  the local continuum intensity. In the second method all the values of the Stokes-V profile as set out by Martínez Pillet et al. (2011) are considered. The second method was adapted to account for the actual number  $n$  of spectral points sampled during the observations. In particular, we applied the formula

$$\text{CP2} = \frac{1}{n \langle I_c \rangle} \sum_{i=1}^n \epsilon_i |V_i|, \quad (2)$$

where  $\epsilon = 1$  for the spectral positions of the line sampling on the blue wing of the line,  $\epsilon = -1$  for the spectral positions on the red wing, and  $\epsilon = 0$  for the line center position;  $n = 21$  is the number of sampled spectral positions; and  $i$  runs from the 1st to the 21st wavelength position. The values  $\langle I_c \rangle$  and  $V_i$  are the average line continuum intensity in a quiet-Sun region within the FOV and of the Stokes-V parameter at the wavelength position  $i$ .

We also estimated the LP signal via the method set out by Martínez Pillet et al. (2011), using the formula

$$\text{LP} = \frac{1}{n \langle I_c \rangle} \sum_{i=1}^n \sqrt{Q_i^2 + U_i^2}, \quad (3)$$

where  $Q_i$  and  $U_i$  are the values of the Stokes-Q and Stokes-U parameters at the wavelength position  $i$ .

The NCP, which is a measure of the asymmetry of the Stokes-V polarization signal, was estimated from the integral of the measured Stokes-V profile following Solanki & Montavon (1993). In particular, we applied the formula

$$\text{NCP} = \int_{\lambda_1}^{\lambda_n} d\lambda V(\lambda), \quad (4)$$

where  $\lambda$ ,  $\lambda_1$ , and  $\lambda_n$  represent the wavelength, and the wavelengths at the 1st and 21st spectral positions of the sampled line, respectively. We computed  $V_{\text{los}}$  by using the phase cross-correlation of Fourier transform as set out in Sect. 2.4 of Schlichenmaier & Schmidt (2000).

The Level 1.5 data were computed by utilizing the Matplotlib (Hunter 2007), Scipy (Virtanen et al. 2020), and Numpy (Harris et al. 2020) libraries written in Python. At present, there are 14 different series of Level 1.5 data available in the archive.

Finally, the Level 1 series from spectropolarimetric observations at the Fe I 6173 Å line were further considered to generate Level 2 data. In particular, all the scans of the above series were processed with inversion techniques. The core of these techniques relies on the inference of the dynamic, magnetic, and thermodynamic properties of the imaged atmosphere from the measured Stokes profiles of single or multiple spectral lines that form at different heights in the solar atmosphere. This is achieved by solving the radiative transfer equation through codes aimed at working the inverse problem (del Toro Iniesta & Ruiz Cobo 2016). The Level 2 data in IBIS-A were obtained with the Very Fast Inversion of the Stokes Vector code (VFISV, Borrero et al. 2011), version 4.0, which performs a Milne-Eddington inversion of measured Stokes profiles. At present, 31 data series have been inverted and a total of 2902 scans processed, which let more than 80% of the calibrated Fe I 6173 Å line observations stored in the archive to also be available as Level 2 data.

The FOV size of Level 1 data<sup>3</sup> is  $500 \times 1000$  pixels<sup>2</sup>, while the science-ready Level 1.5 and 2.0 data both cover  $350 \times 800$  pixels<sup>2</sup>, or  $\approx 34 \times 78$  arcsec<sup>2</sup>.

### 3. IBIS-A data

The IBIS observing campaigns varied depending on instrumental setup, observer, target, and science goals, thus the acquired data are heterogeneous. However, almost all the IBIS datasets include the sampling of a photospheric line and a chromospheric line, either Ca II 8542 Å or H $\alpha$  6563 Å, and sometimes both. From 2013 to 2017 the chromospheric Ca II 8542 Å observations were frequently carried out in spectropolarimetric mode.

Figure 2 summarizes the main characteristics of the IBIS data available in IBIS-A. Figure 2 panels a and b show the fraction of spectroscopic and spectropolarimetric series, and the spectral lines sampled in the observations, respectively. The spectropolarimetric data are 37% of the available measurements (in terms of number of sets). Over 19%, 6%, and 4% of the data refer to the photosphere sampled at the Fe I 6173 Å, Fe I 6302 Å, and Na I 5896 Å lines, respectively; 38% and 27% of the data report observations of the chromosphere at the Ca II 8542 Å and H $\alpha$  6563 Å lines, respectively. Figure 2 panels c and d display the fraction of sequences in the archive depending on their duration and solar disk position of the target, respectively. Almost 56% of the data consist of sequences of observations lasting less than 30 min, but more than 12% of the available data report on long-duration observations exceeding 1 h. In addition, it is worth noting that “duration” in these statistics refers to the length of the individual series. However, sometimes multiple series were run with minimal delay between them, and could thus be considered a continuous observing block. About 53% of the observations were taken at disk center ( $\mu > 0.85$ , where  $\mu = \cos\theta$  and  $\theta$  is the heliocentric angle), while over 40% of the data image the solar

<sup>2</sup> Interactive Data Language, Harris Geospatial Solutions, Inc.

<sup>3</sup> Currently available only for spectropolarimetric series.

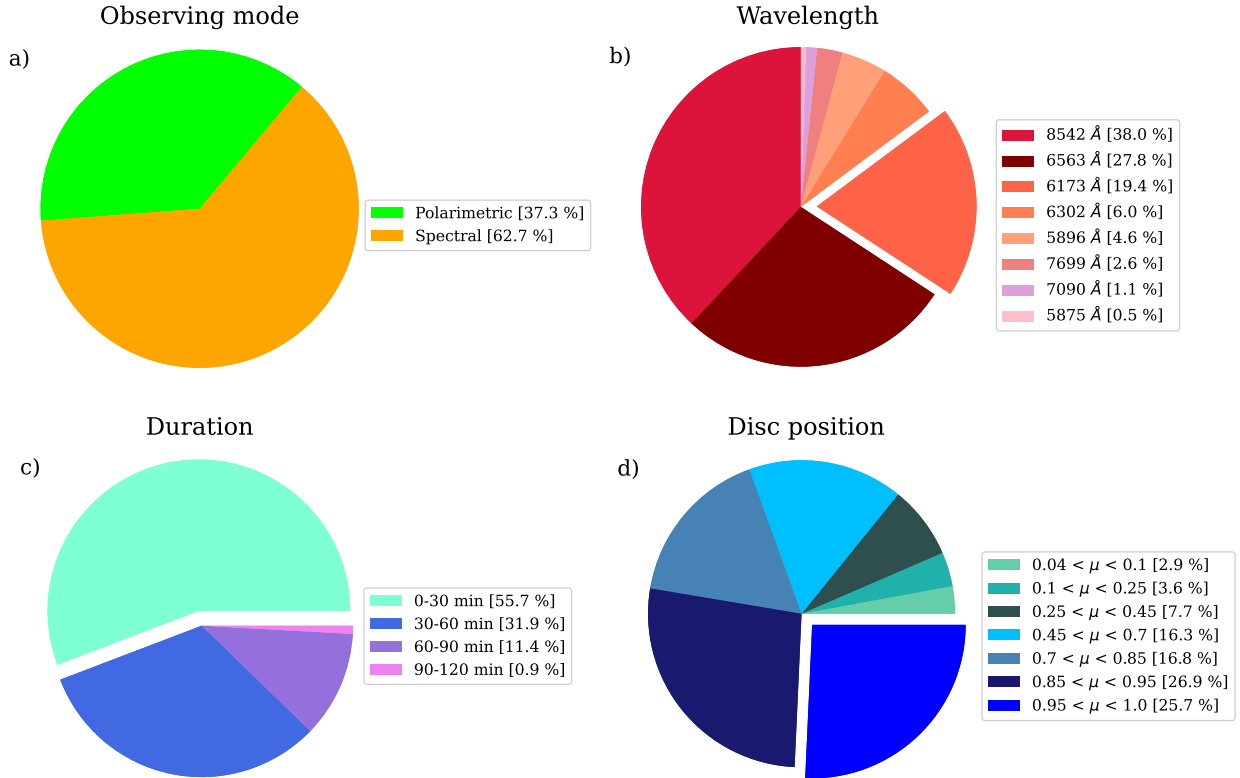


**Fig. 2.** Level 0 data stored in the archive. Shown are pie charts of the fraction (in %) of *panel a)* the spectroscopic and spectropolarimetric data available in IBIS-A, *panel b)* the spectral lines (in Å) acquired during the observations, *panel c)* the duration (in minutes) of the observational sequences, and *panel d)* the  $\mu$  disk position of the FOV ( $\mu = \cos\theta$  where  $\theta$  is the heliocentric angle).

atmosphere at intermediate disk locations ( $0.25 < \mu < 0.85$ ) and about 4% very close to the limb ( $0.04 < \mu < 0.1$ ) or above it.

Figure 3 (top panel) describes the IBIS-A data in terms of the median value of the “quality image” parameter  $q$ . This quantity is a measure of the image resolution in arcsec due to the seeing. It is generated by the DST control system by monitoring the variability of the intensity of the Sun’s light during the observing run (see Seykora 1993 for more details). Figure 3 shows that more than 77% of the IBIS-A data were taken under very good and average seeing conditions (i.e., image resolution  $< 1$  arcsec), while about 4% of the observations are of the solar atmosphere at medium spatial resolution with image resolution  $> 1.5$  arcsec. About 18% of the data are characterized by a resolution in the range 1–1.5 arcsec.

Figure 3 (bottom panel) provides information on the homogeneity of the datasets available in the archive. Here we show the number of datasets depending on the homogeneity of the image quality parameter  $q$  during the observing run, for observations of given duration  $d$ . The distribution of values in Fig. 3 (bottom panel) shows that a large fraction of the short duration datasets available in IBIS-A were taken under stable excellent and good seeing conditions, but this also holds for a significant number of observations exceeding 1 h.

### 3.1. Data format

IBIS-A includes the data generated by the instrument, those processed for instrumental calibration and seeing restoration, and those further elaborated to derive physical quantities and science-ready data. These diverse sets, which form the Level 0, Level 1, Level 1.5, and Level 2 data, respectively, are stored in the archive with different formats.

The Level 0 data ( $\approx 25$  TB of data) are archived as extended FITS format files in a main folder comprising two subdirectories. These include the NB and BB data, respectively, containing data for both science and instrumental calibrations. The name of the files describes the nature of the data (e.g., Science, Dark, Flat-Field). Each file comprises the data from a single iteration of all pre-filters and wavelengths used during observations. General information about the data, which is common to the whole observing run, is stored in the primary FITS header, while information specific to a single exposure (e.g., acquisition time, wavelength position, exposure time, telescope pointing, polarization state) is stored in the extended FITS headers. Figures A.1 and A.2 give examples of such information. Each FITS file consists of a four-dimensional array with  $(x, y, \lambda, \text{Pol})$ -axes, where the spatial  $x$ - and  $y$ -axes describe the instrument FOV, the  $\lambda$ -axis covers the wavelength spectral points along the sampled line, and the Pol-axis represents the six polarimetric states (I+Q, I-Q, I+V, I-V, I+U, and I-U) measured by the instrument. The above structure and labeling of the Level 0 data follow the IBIS data definition and file arrangement given at the DST.

Table 1 gives an overview of the Level 0 data currently available in IBIS-A, with information on the number of datasets, and the fraction of observations depending on the target and on sampled spectral lines. The information is provided per year from 2012 to 2019. Table 1 shows that there is a variety of observations at different lines, and targets available in IBIS-A, the latter including quiet Sun, sunspot, pore, and limb regions. Some of the data also relate to plages and filaments.

The Level 1 data ( $\approx 4$  TB of data) are stored in the archive using the .sav format generated by the IDL pipeline applied to the Level 0 observations. The Level 1 files consist of four-dimensional arrays with  $(x, y, \lambda, \text{Stokes})$ -axes, where the spatial

**Table 1.** Overview of the Level 0 data available in IBIS-A.

Year	N series	PO	Target <sup>(a)</sup> (%)				N datasets for each spectral line <sup>(b)</sup>							
			SP	QS	L		K I 7699	Fe I 6173	Ca II 8542	H $\alpha$ 6563	Fe I 630.2	Fe I 7090	Na I D1 5896	He I 5875
2012	33	51.5	30.3	15.2	0	0	33	33	0	33	0	0	0	
2013	81	8.7	48.1	28.4	14.8	0	25	52	31	0	4	5	0	
2014	64	14.1	54.2	10.3	20.4	0	45	27	52	0	7	0	5	
2015	45	28.8	46.7	24.4	0	0	37	40	21	16	0	0	0	
2016	26	19.2	46.2	34.6	0	0	17	26	17	0	0	1	0	
2017	20	40	35	25	0	0	16	20	10	10	0	4	0	
2018	136	8.8	0.7	69.8	20.6	25	14	127	104	0	0	27	0	
2019	47	32	0	63.4	4.3	0	1	46	37	0	0	8	0	

**Notes.** <sup>(a)</sup>PO: pore, SP: sunspot, QS: quiet sun, L: Limb region. <sup>(b)</sup>Line core is given in Å.

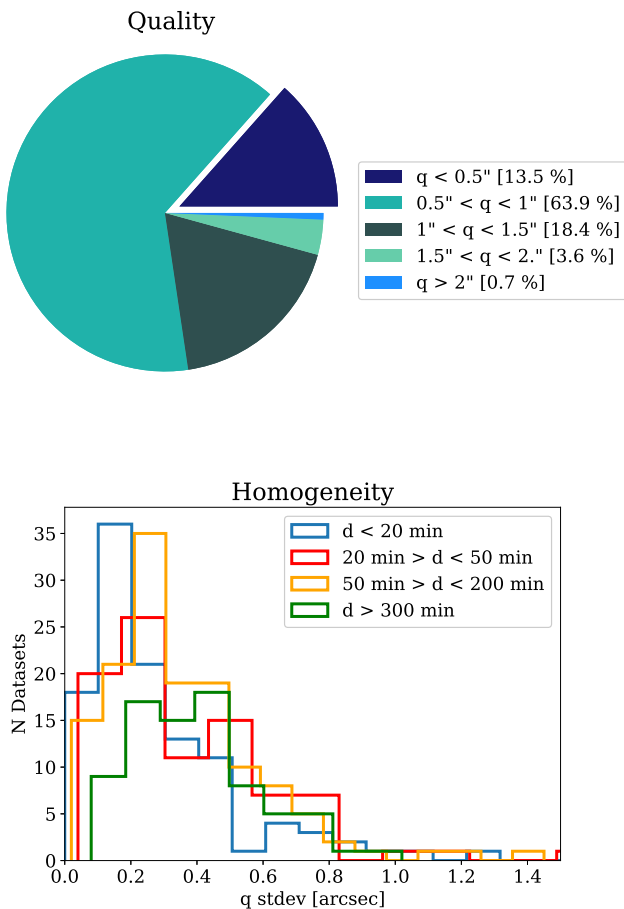


**Fig. 3.** Quality and homogeneity of the Level 0 data stored in the archive. *Top panel:* pie chart of the IBIS-A data divided for the median value of the quality image parameter  $q$  (in arcsec) during acquisition of Level 0 data (see Sect. 3.1 for details). *Bottom panel:* number of Level 0 datasets depending on their duration  $d$  and homogeneity of the quality image parameter  $q$  during observations. The homogeneity of the dataset is described by the standard deviation of the  $q$  values measured during the observing run.

$x$ - and  $y$ -axes describe the instrument FOV, the  $\lambda$ -axis renders the wavelength of the line sampling during the observation, and the Stokes-axis represents the (I, Q, U, V) polarimetric states of the measurements. Each Level 1 file also contains information about the data in the `info_nb` variable, which is a structure with

several tags and values. Figure A.3 lists the fields included in the `info_nb` variable. The Level 1 data are stored with the naming convention `llll-nbsss.pc.sav` and `llll-nbsss.sav` for the spectropolarimetric and purely spectroscopic data, respectively, where “llll” is the wavelength (in Å) and “sss” is the scan number in the corresponding Level 0 data. Each `.sav` file thus reports the data at the given time  $t$  of the “sss” scan during the sequence of observations. The structure and naming of the Level 1 data follow those set in the NSO calibration pipeline.

Table A.1 summarizes the main information of the Level 1 data currently available in IBIS-A, with details on targets, lines and number of spectral points sampled during observations, number of measurements at each spectral point, and number of line scans. Table A.1 makes it clear that most of these data currently include observations of the chromosphere at the Ca II 8542 Å and H $\alpha$  6563 Å lines. It is worth noting that the Level 1 data of IBIS-A can be accessed with the CRISP SPectral EXplorer (CRISPEX) graphical user interface (Vissers & Rouppe van der Voort 2012; Löfdahl et al. 2021), version 1.7.4, which was developed to manage the CRISP and CHROMIS data. For this purpose the IBIS data format needs to be adapted to the FITS format accepted by the CRISPEX interface with a code available at the IBIS-A site specified in the following. The pipeline to reduce Level 0 data is also available at the archive site. Other codes are available (e.g., to convert Level 1 data from `.sav` to `.FITS` format).

The Level 1.5 and Level 2 data ( $\approx 15$  GB and 20 GB of data, respectively) are stored in the archive in FITS format files<sup>4</sup> as multi-dimensional arrays with ( $x$ ,  $y$ , var)-axes, where  $x$  and  $y$  are the spatial coordinates in the FOV, and var indicates the physical quantities derived from the line measurements and VFISV data inversion. The physical quantities obtained from line measurements include estimates of the CP<sup>5</sup>, LP, NCP, and  $V_{\text{los}}$ , while those from the VFISV data inversion comprise the magnetic field strength ( $B$ ), the inclination ( $B_{\text{inc}}$ ) and azimuth ( $B_{\text{azi}}$ ) angles of the magnetic field, the longitudinal component of the velocity field ( $V_{\text{los}}$ ), and the magnetic filling factor ( $F_{\text{fact}}$ ). The field azimuth ambiguity is unresolved.

The Level 1.5 and Level 2 data comprise metadata information in the form of FITS header keywords that are stored in a primary header and two extended headers. The primary header contains information derived from the Level 0 data to describe the observations with regard to telescope pointing as Stonyhurst Heliographic solar coordinates (in degrees);

<sup>4</sup> At present, FITS Standard Version 3 using CFITSIO Version 3.47.

<sup>5</sup> From both of the above-mentioned calculations applied.

**Table 2.** Overview of the Level 1.5 and Level 2 data available in IBIS-A.

Date YY-MM-DD	Time (UT)	Target <sup>(a)</sup>	Scans	$\mu$ <sup>(b)</sup>	Cadence (s)	Data <sup>(c)</sup> processed	Other data <sup>(c)</sup> available	Ref	Level <sup>(d)</sup>
2012-04-17	13:58:43	PO	56	0.94	67	Fe I 6173	Fe I 6302, Ca II 8542 (I)	1	2.0
2012-04-17	15:09:06	PO	68	0.94	67	Fe I 6173	Fe I 6302, Ca II 8542 (I)		2.0
2012-04-17	18:43:40	PO	100	0.94	67	Fe I 6173	Fe I 6302, Ca II 8542 (I)		2.0
2013-10-07	17:39:08	SP	130	0.96	33	Fe I 6173	Na I D1 5896		2.0
2014-04-21	14:15:33	PO	15	0.98	116	Fe I 6173	Ca II 8542		2.0
2014-10-14	15:15:57	PO	238	0.44	50	Fe I 6173	Ca II 8542, H $\alpha$ 6563 (I)		2.0
2015-04-10	14:34:25	SP	237	0.88	23	Fe I 6173	Ca II 8542		2.0
2015-04-11	14:14:40	PO	19	0.69	131	Fe I 6173	Ca II 8542		2.0
2015-04-11	15:01:55	PO	18	0.88	131	Fe I 6173	Ca II 8542		2.0
2015-04-30	13:52:44	QS	290	1.00	27	Fe I 6173	Ca II 8542 (I)		2.0
2015-05-01	14:17:52	QS	58	1.00	48	Fe I 6173, Ca II 8542		2	1.5, 2.0
2015-05-02	14:25:34	QS	50	1.00	44	Fe I 6173, Ca II 8542			1.5, 2.0
2015-05-02	15:08:33	QS	20	0.99	44	Fe I 6173, Ca II 8542			1.5, 2.0
2015-05-02	15:27:31	QS	79	0.98	44	Fe I 6173, Ca II 8542			1.5, 2.0
2015-05-03	14:28:42	SP	85	0.74	44	Fe I 6173, Ca II 8542			1.5, 2.0
2015-05-03	17:15:05	SP	25	0.75	44	Fe I 6173, Ca II 8542			1.5, 2.0
2016-05-13	13:38:48	SP	50	0.67	42	Fe I 6173, Ca II 8542			1.5, 2.0
2016-05-13	14:15:05	SP	58	0.67	42	Fe I 6173, Ca II 8542			1.5, 2.0
2016-05-13	15:00:27	PO	163	0.88	42	Fe I 6173, Ca II 8542			1.5, 2.0
2016-05-19	13:37:43	SP	100	0.98	42	Fe I 6173, Ca II 8542			1.5, 2.0
2016-05-20	13:53:06	SP	319	0.99	48	Fe I 6173, Ca II 8542		3, 4, 5	1.5, 2.0
2016-10-11	16:04:17	QS	29	1.00	49	Fe I 6173	Ca II 8542, H $\alpha$ 6563 (I)		2.0
2016-10-11	16:33:07	QS	31	1.00	49	Fe I 6173	Ca II 8542, H $\alpha$ 6563 (I)		2.0
2016-10-12	14:53:30	QS	100	1.00	49	Fe I 6173	Ca II 8542, H $\alpha$ 6563 (I)		2.0
2017-05-05	14:06:00	PO	85	0.82	40	Fe I 6173, Ca II 8542			1.5, 2.0
2017-05-05	15:37:49	QS	107	0.81	40	Fe I 6173, Ca II 8542			1.5, 2.0
2017-05-12	13:34:16	QS	40	1.00	40	Fe I 6173, Ca II 8542			1.5, 2.0

**Notes.** <sup>(a)</sup>Target: PO: pore, SP: sunspot, QS: quiet sun. <sup>(b)</sup> $\mu$  :  $\mu = \cos\theta$ , where  $\theta$  is the heliocentric angle. <sup>(c)</sup>Spectral lines observed with IBIS. Line core is given in Å. (I) specifies spectroscopic data. <sup>(d)</sup>Level: 1.5 and 2.0 science-ready data described in the main text.

**References.** 1: Ermolli et al. (2017), 2: Murabito et al. (2020b), 3: Stangalini et al. (2018), 4: Murabito et al. (2019), 5: Houston et al. (2020).

solar P0, L0, B0 ephemeris (in degrees); apparent solar photospheric disk radius (in arcsec); Seykora scintillation monitor value (the quality image parameter, in arcsec); and duration of the line scan (in seconds). The information stored in the first and second extended headers is related to the physical quantities available in the data and spectral sampling of the observations employed to estimate them, respectively. Since the Level 1.5 data are obtained from observations taken at the Fe I 6173 Å and Ca II 8542 Å lines, the second extended header of Level 1.5 data includes information on both the sampled lines, while it only refers to Fe I 6173 Å spectral measurements for Level 2 data. It is worth noting that the metadata information delivered in the Level 1.5 and Level 2 data is compliant with the SOLARNET recommendations (Haugan & Fredvik 2015, 2020). In particular, a number of keywords employed in the primary and extended headers address the SOLARNET recommendations: date and time of data series, wavelength, observing mode, exposure time, instrument and telescope employed, frame dimension, solar ephemeris, telescope pointing, data author, data version, name of the procedures applied to the data, origin, and level of the data.

Figures A.4, A.5, and A.6 give examples of keywords in the FITS header of the Level 1.5 and Level 2 data. Level 1.5 and Level 2 files are stored in the archive with the naming convention *IBIS\_l\_YYYYMMDD\_HHMMSS*, where “l” shows the data level, and *YYYYMMDD* and *HHMMSS* the date and time

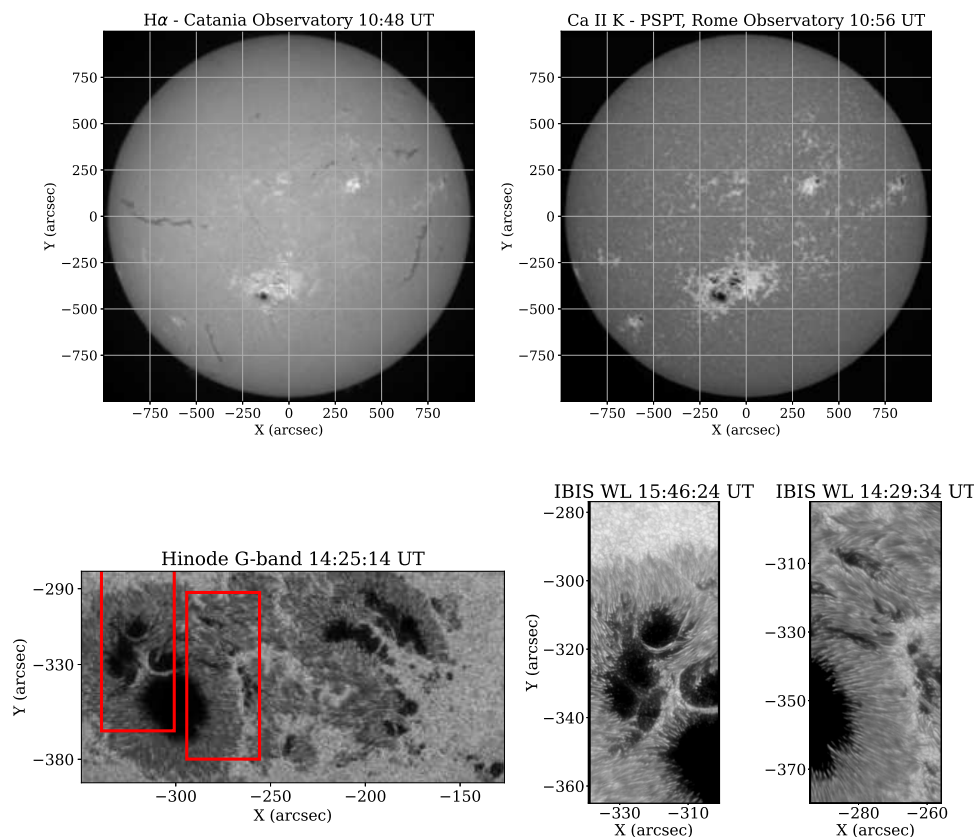
of the related observations. This file naming convention also addresses the SOLARNET recommendations.

Table 2 summarizes the main characteristics of the Level 1.5 and Level 2 data available in IBIS-A. There is a variety of targets in science-ready data, including pore, sunspot, and quiet-Sun regions. In addition, a few series have further co-temporal observations available in addition to the Fe I 6173 Å and Ca II 8542 Å observations considered to produce the Level 1.5 and Level 2 data, obtained at the photospheric Fe I 6302 Å and chromospheric H $\alpha$  6563 Å lines. Table A.2 summarizes the information on the Level 2 data currently available in IBIS-A and further co-temporal spectral lines observed with IBIS.

### 3.2. Contextual and coordinated observations

The data stored at IBIS-A are characterized by the large volume of each target observation and the challenging analysis that is typical of any spectropolarimetric measurements. Nevertheless, the literature is rich in novel results derived from the analysis of data either belonging to or similar to those in IBIS-A. Almost all these studies, as well as the ones listed in Sect. 1, clearly show that combining spectropolarimetric measurements such as those in IBIS-A with data from other instruments greatly enhances the return of the scientific analysis of these observations by expanding the FOV and range of atmospheric heights that can be investigated. In this light, the IBIS-A archive offers





**Fig. 4.** Examples of contextual data available in IBIS-A. Full-disk observations of the solar chromosphere acquired on 22 October 2014 at the  $H\alpha$  (top left) and Ca II K (top right) lines by the INAF Catania and Rome/PSPT telescopes, respectively, and a zoom-in on the Hinode/SOT observation (Level 1) of the central region of NOAA AR 12192 (bottom left), also imaged by the IBIS data available in IBIS-A (bottom right).

its users links to observations complementary to the IBIS series available in the archive, such as those from co-temporal and near co-temporal high-resolution observations of the solar atmosphere available from the instruments on board the Hinode/SOT (Tsuneta et al. 2008) and IRIS (De Pontieu et al. 2014) satellites, and full-disk filtergrams from INAF solar telescopes (Ermolli et al. 2011; Romano et al. 2022).

Figure 4 shows examples of contextual data available in IBIS-A for the IBIS dataset obtained on 22 October 2014 observing the active region (AR) NOAA 12192. The contextual data include full-disk observations of the solar photosphere (not shown) and chromosphere at the  $H\alpha$  6563 Å and Ca II K 3933 Å lines acquired by the INAF Catania and Rome/PSPT telescopes on the same day as the IBIS observations, and a magnification of the central region of AR NOAA 12192 from Hinode/SOT observations almost co-temporal with the IBIS measurements stored in IBIS-A. The latter pertain to the inner part of the AR during the occurrence of a X1.6 flare. It is worth noting that at present users are only provided with direct links to the Hinode/SOT and IRIS data complementary to those available for each series in IBIS-A, without any processing, for example to scale and target observations from the diverse instruments.

#### 4. Data access

The IBIS-A data are stored on a RS24S3 SuperNAS server (96 TB, 64 GB Ram, 2 CPU Haswell 4C E5-2623V3 3G) at the INAF Osservatorio Astronomico di Roma<sup>6</sup>.

<sup>6</sup> The IBIS-A data can be accessed at <http://ibis.oa-roma.inaf.it/IBISA/>

The metadata of the Level 0 files were incorporated into a MySQL database (DB) by using a Python application. The Python Django framework was used both to define the relational table schema using its object-relational internal mapping and to provide the web pages with simple query search interface.

The IBIS-A archive, so built, works on the server running Python 2.7.6, with Django version 1.9.1 on a MySQL 5.5 server. It has recently been tested (to update the query service) on a test machine running Python 3.9.1, Django 3.2.9, and a MySQL 8.0 server.

The interface permits data to be searched according to various criteria: solar target, disk position, observational mode, data range. The criteria can be combined in order to refine searches. Based on the metadata stored on the IBIS-A DB, the data search dynamically generates a HTML page with information about the available data. The HTML tabular output is prepared using Django views for the search results and formatted in HTML using the internal Django template tools. The products of the data search also include movies and plots of the atmospheric seeing during observations, as basic information to allow users to assess the data quality. The movies for quick-look purposes were created by using the 2D plotting library Matplotlib (version 1.5.2).

Browsing IBIS-A does not require authentication, but users have to register and log in to be able to request and download IBIS-A data.

#### 5. A glimpse at science with IBIS-A

A significant fraction of the observations stored in IBIS-A are still scientifically unexplored. Figure 5 displays examples

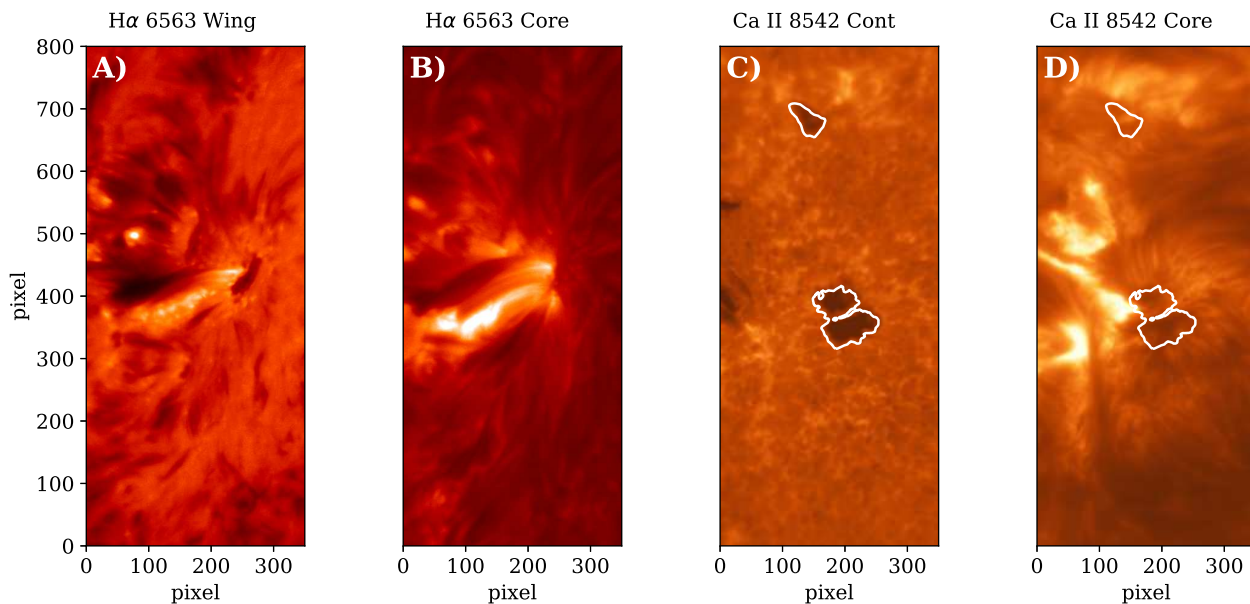


**Fig. 5.** Examples of Level 1 data of chromospheric flaring regions available in IBIS-A. The data were acquired along the  $H\alpha$  6563 Å line, in the wing (*panel A*) and core (*panel B*) of the line, on 10 October 2014, 14:20 UT at disk position  $\mu = 0.43$ , and along the Ca II 8542 Å line, in the far wing (*panel C*) and line core (*panel D*), on 13 May 2016, 15:00 UT, at disk position  $\mu = 0.9$ . The white lines in the rightmost panels show contours of the magnetic pore regions corresponding to  $I_c(x, y) = 0.8 \times I_c$  (quiet), where  $I_c(x, y)$  and  $I_c$  (quiet) are values of the line continuum intensity at the given position  $(x, y)$  and in the quiet region.

of these data. They concern calibrated observations of flaring regions obtained at the photospheric Fe I 6173 Å line and at the chromospheric  $H\alpha$  6563 Å line (the latter is shown in Fig. 5 panels A and B at two different wavelengths) and Ca II 8542 Å line (Fig. 5 panels C and D) on 10 October 2014, 14:25 UT and 13 May 2016, 15:00 UT, at disk positions  $\mu = 0.47$  and  $\mu = 0.89$ , respectively. The observations of these flaring regions exceed 100 min each.

The atmosphere imaged in the wing of Ca II 8542 Å (Fig. 5 panel C) is typical of the middle photosphere, with a clear pattern of reversed granulation. Instead, the wing of  $H\alpha$  6563 Å, and the core of both  $H\alpha$  6563 Å and Ca II 8542 Å (Fig. 5 panels A, B, D) show various parts of the chromosphere, with the typical dazzling variety of features such as surges, bundles of arch filament systems, spicules, and localized and extended bright regions. Figure 6 shows science-ready data available in IBIS-A for the flaring region with pores shown in panels C and D of Fig. 5. On the left side of the FOV, the maps of CP derived from the photospheric Fe I 6173 Å and chromospheric Ca II 8542 Å data (Fig. 6 panels F and G, respectively), and the map of the field inclination obtained from the VFISV data inversion (Fig. 6 panel D) reveal magnetic field concentrations with opposite polarity with respect to that in the pores. At the same location, the chromospheric observations at the Ca II line core (Fig. 5 panel D) display a filament and a footpoint of the flaring region (see  $X = [0, 100]$ ,  $Y = [300, 400]$ ). Magnetic signatures of these structures are also found in the chromospheric CP map from Ca II 8542 Å data (Fig. 6 panel G). The maps of the magnetic field strength derived from inversion of the photospheric Fe I 6173 Å data (Fig. 6 panels B, C, and A, respectively) show values up to 1.4 kG in the pores and field strength in the range of 0.4–0.6 kG in their surrounding area. There the maps of the photospheric LP and  $V_{\text{los}}$  from the Fe I 6173 Å data (Fig. 6 panels E and H, respectively) show horizontal magnetic fields and velocity fields with strong upflows.

Figure 7 gives examples of the Level 1, Level 1.5, and Level 2 data available in IBIS-A for the spectropolarimetric observations of a sunspot region shown in Fig. 1. That region was observed on 13 May 2016, 15:38 UT at disk position  $\mu = 0.67$ . It is worth noting that both Figs. 6 and 7 show values of the field inclination derived from data inversion in quiet-Sun areas peaked around  $90^\circ$ . As reported by Borrero & Kobel (2011), these values result from the inversion of LP measurements characterized by a signal-to-noise ratio lower than 4.5. However, a more accurate estimate of the magnetic field inclination in quiet Sun regions is beyond the scope of the present work, which aims to provide quick-look science-ready data to IBIS-A users.

## 6. Summary and conclusions

This paper presents the IBIS-A archive, which currently includes 30TB of data taken with the Interferometric BIdimensional Spectropolarimeter (IBIS) during 28 observing campaigns carried out from 2008 to 2019 over 159 days. This presentation of the archive is meant to facilitate and foster the scientific usage of the IBIS-A data with examples of the data quality and their application in recent and undergoing studies relevant to solar processes and space weather science.

Since the implementation of IBIS-A in 2016, the raw data available in the archive have increased, as has the fraction of calibrated measurements. In addition, links have been added pointing to complementary data of the solar atmosphere available from coordinated measurements performed with the instruments on board the Hinode and IRIS satellites, and the full-disk red continuum, Ca II K, and  $H\alpha$  observations of the photosphere and chromosphere from the INAF synoptic solar telescopes.

Furthermore, the archive has been populated with higher level products from inversion of the calibrated data. Multi-dimensional arrays with maps of circular, linear, and net circular polarization, and  $\text{los}$  velocity patterns from calibrated photospheric Fe I 6173 Å and chromospheric Ca II 8542 Å series

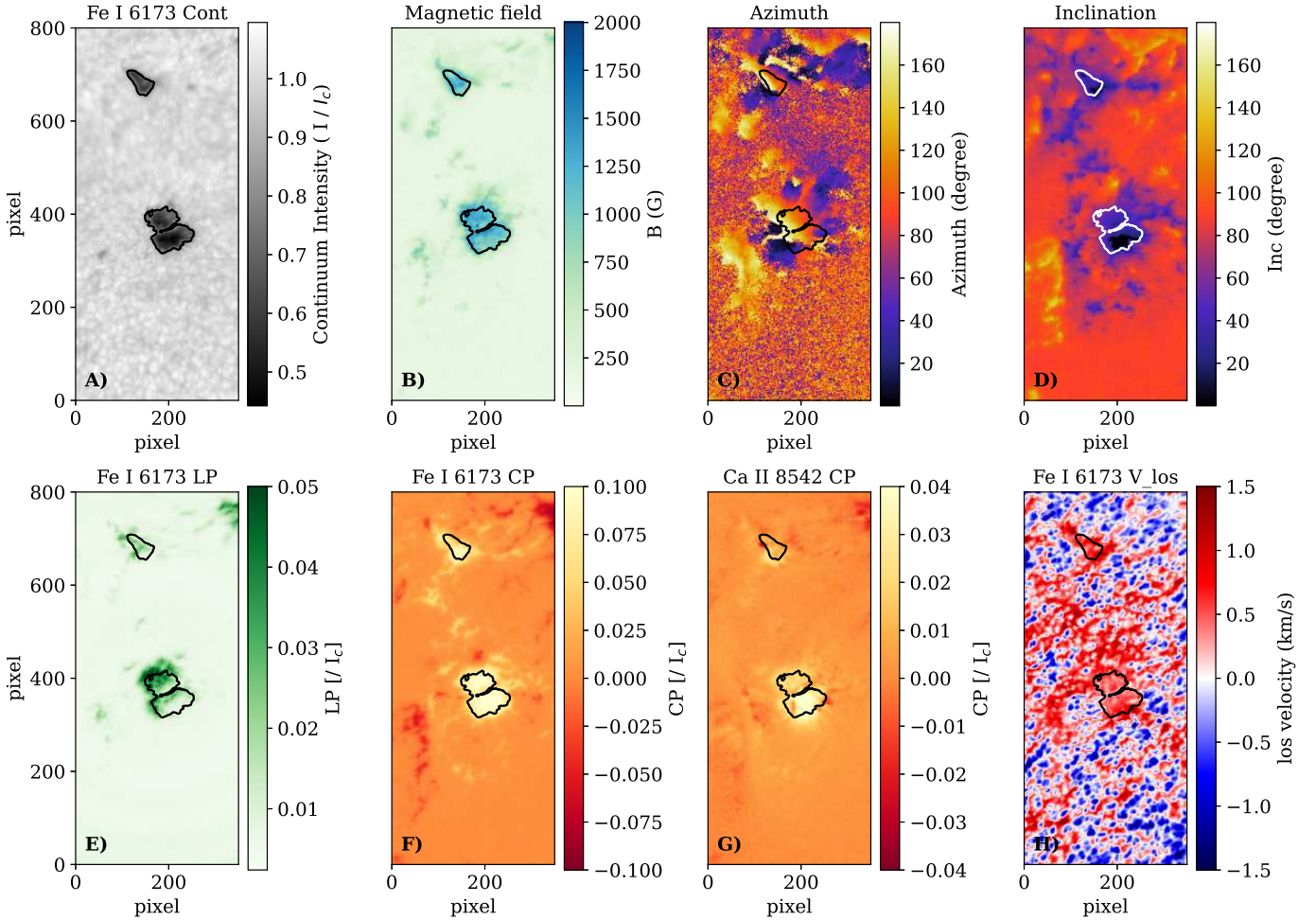


**Fig. 6.** Examples of Level 1, Level 1.5, and Level 2 data available in IBIS-A for the flaring region with magnetic pores shown in Fig. 5. The observations were taken on 13 May 2016 at 15:00 UT. The *top panels* show Level 1 (*panel A*) and Level 2 (*panels B–D*) data, while the *bottom panels* show Level 1.5 (*panels E–H*) data. *Top panels, from left to right:* maps of the intensity measured on the FOV at the Fe I 6173 Å line continuum and of the magnetic field strength, azimuth, and inclination angles derived from the VFISV inversion of the Fe I 6173 Å line data. *Bottom panels, from left to right:* maps of the linear and circular polarization estimated from the photospheric Fe I 6173 Å line data, circular polarization from the chromospheric Ca II 8542 Å observations, and *los* velocity field at photospheric heights from Fe I 6173 Å measurements (see Fig. 5 for more details).

are also offered to registered users. In addition, more than 80% of the calibrated Fe I 6173 Å photospheric series have already been inverted with the VFISV code to offer a quick-look view of the magnetic and velocity fields in the archived targets. A further milestone will be reached by the inversion of the remaining photospheric data and of the chromospheric series with the new NLTE DeSIRE code (Ruiz Cobo et al. 2022). The IBIS-A team will also incorporate more data in the archive when they become available.

The IBIS-A data include metadata for proper interpretation and archiving of the observations available in the archive. At present, the keywords employed in the header of FITS Level 1.5 and Level 2 data are partly compliant<sup>7</sup> with the recently formulated SOLARNET recommendations. The complete standardization of the metadata information provided by the IBIS-A data planned in the near future will facilitate their usage by users with limited knowledge of the spectropolarimetric observations. In addition, it will allow easy inclusion of IBIS-A data in future Solar Virtual Observatories.

<sup>7</sup> Following the definition in relevant documents.

IBIS-A represents a unique resource for investigating the plasma processes in the solar atmosphere and the solar origin of Space Weather events. In addition, it represents the prototype of the archive that will host the data acquired with the updated version of the IBIS instrument, named IBIS 2.0, which is under development for installation at the Observatorio del Roque de Los Muchachos in the Canary Islands.

Browsing IBIS-A does not require authentication, but users have to register and log in to be able to request and download data. The IBIS-A team is open for technical support and help with the data analysis to foster the use of data stored in the archive in new science projects. In this respect, we note that IBIS-A is currently maintained by the H2020 SOLARNET High-resolution Solar Physics Network project, which aims at integrating the major European infrastructures in the field of high-resolution solar physics. Therefore, any publication that uses data contained in IBIS-A should acknowledge the above support by reporting “This study makes use of data collected in the IBIS-A archive, which has received funding from the European Union’s Horizon 2020 research and innovation programme under Grant Agreements No. 824135 (SOLARNET).”

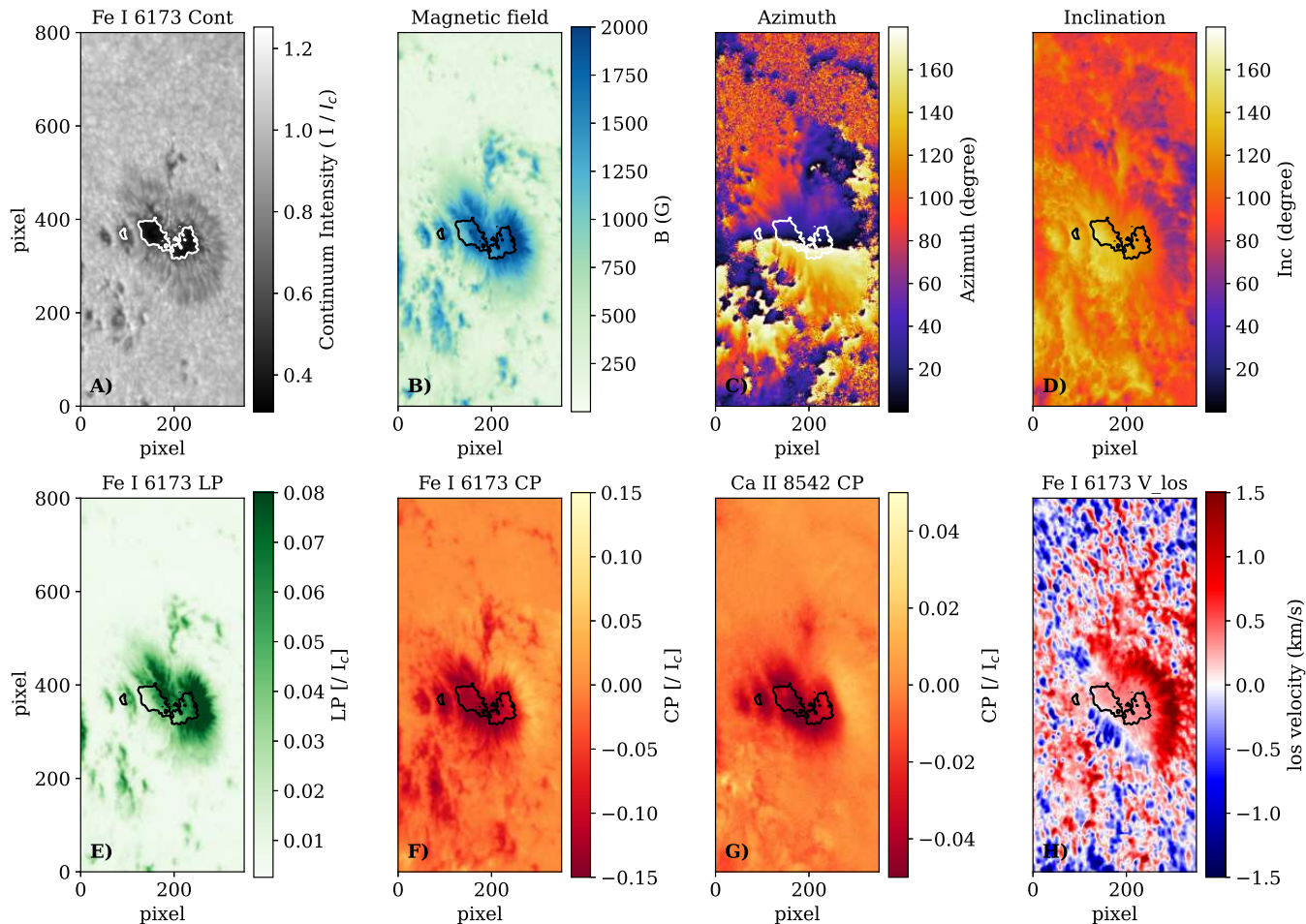


**Fig. 7.** Examples of Level 1, Level 1.5, and Level 2 data available in IBIS-A for the sunspot region observed on 13 May 2016, 13:38 UT at disk position  $\mu=0.68$  shown in Fig. 1. The *top panels* show Level 1 (*panel A*) and Level 2 (*panels B–D*) data, while the *bottom panels* show Level 1.5 (*panels E–H*) data (see Figs. 5 and 6 for more details).

**Acknowledgements.** The authors thank Doug Gilliam and Mike Bradford for acquisition of IBIS data throughout the years. They also thank Juan Manuel Borrero and Han Uitenbroek for their work on IBIS data. The authors are grateful to the referee for carefully reading of the paper and for her/his comments. This research has received funding from the European Union’s FP7 Capacities program under grant agreement No 312495 (SOLARNET) and from the European Union’s Horizon 2020 Research and Innovation program under grant agreements No 824135 (SOLARNET) and No 739500 (PRE-EST). This work was also supported by the Italian MIUR-PRIN grant 2017 “Circumterrestrial Environment: Impact of Sun–Earth Interaction” and by the INAF Istituto Nazionale di Astrofisica. The Level 2 data available in IBIS-A were obtained from access to servers of the Italian CINECA and INAF. IBIS has been designed and constructed by the INAF Osservatorio Astrofisico di Arcetri with contributions from the Università di Firenze, the Università di Roma Tor Vergata, and upgraded with further contributions from National Solar Observatory (NSO) and Queens University Belfast. IBIS was operated with support of the NSO. The NSO is operated by the Association of Universities for Research in Astronomy, Inc., under cooperative agreement with the National Science Foundation. This research made use of NASA’s Astrophysics Data System.

## References

- Abbasvand, V., Sobotka, M., Heinzel, P., et al. 2020, *ApJ*, **890**, 22  
 Baker, D., Stangalini, M., Valori, G., et al. 2021, *ApJ*, **907**, 16  
 Bellot Rubio, L., & Orozco Suárez, D. 2019, *Liv. Rev. Sol. Phys.*, **16**, 1  
 Blandford, R., Meier, D., & Readhead, A. 2019, *ARA&A*, **57**, 467  
 Borrero, J. M., & Kobel, P. 2011, *A&A*, **527**, A29  
 Borrero, J. M., Tomczyk, S., Kubo, M., et al. 2011, *Sol. Phys.*, **273**, 267  
 Borrero, J. M., Jafarzadeh, S., Schüssler, M., & Solanki, S. K. 2017, *Space Sci. Rev.*, **210**, 275  
 Brosius, J. W., Daw, A. N., & Rabin, D. M. 2014, *ApJ*, **790**, 112  
 Cao, W., Gorceix, N., Coulter, R., et al. 2010, *SPIE Conf. Ser.*, **7735**, 77355V  
 Capparelli, V., Zuccarello, F., Romano, P., et al. 2017, *ApJ*, **850**, 36  
 Cauzzi, G., Reardon, K. P., Uitenbroek, H., et al. 2008, *A&A*, **480**, 515  
 Cauzzi, G., Reardon, K., Rutten, R. J., Tritschler, A., & Uitenbroek, H. 2009, *A&A*, **503**, 577  
 Cavallini, F. 2006, *Sol. Phys.*, **236**, 415  
 Cheung, M. C. M., & Isobe, H. 2014, *Liv. Rev. Sol. Phys.*, **11**, 3  
 Collados, M., Bettonvil, F., Cavaller, L., et al. 2013, *Mem. Soc. Astron. Italiana*, **84**, 379  
 Criscuoli, S., & Tritschler, A. 2014, *IBIS Data Reduction Notes*, *Tech. Rep. NS05*, National Solar Observatory, Sacramento Peak  
 Criscuoli, S., Del Moro, D., Giannattasio, F., et al. 2012, *A&A*, **546**, A26  
 Criscuoli, S., Ermolli, I., Uitenbroek, H., & Giorgi, F. 2013, *ApJ*, **763**, 144  
 Del Moro, D., Giordano, S., & Berrilli, F. 2007, *A&A*, **472**, 599  
 del Toro Iniesta, J. C., & Ruiz Cobo, B. 2016, *Liv. Rev. Sol. Phys.*, **13**, 4  
 De Pontieu, B., Title, A. M., Lemen, J. R., et al. 2014, *Sol. Phys.*, **289**, 2733  
 Ermolli, I., Criscuoli, S., & Giorgi, F. 2011, *Contrib. Astron. Observ. Skalnaté Pleso*, **41**, 73  
 Ermolli, I., Cristaldi, A., Giorgi, F., et al. 2017, *A&A*, **600**, A102  
 Ermolli, I., Cirami, R., Calderone, G., et al. 2020, *SPIE Conf. Ser.*, **11447**, 114470Z  
 Giordano, S., Berrilli, F., Del Moro, D., & Penza, V. 2008, *A&A*, **489**, 747  
 Harris, C. R., Millman, K. J., van der Walt, S. J., et al. 2020, *Nature*, **585**, 357  
 Haugan, S. V. H., & Fredvik, T. 2015, Document on Standards for Data Archiving and VO, Deliverable D20.4, SOLARNET (EC 7th FP grant 312495, Tech. Rep. D20.4, Institute of Theoretical Astrophysics, University of Oslo  
 Haugan, S. V. H., & Fredvik, T. 2020, *ArXiv e-prints*, [arXiv:2011.12139]  
 Houston, S. J., Jess, D. B., Keppens, R., et al. 2020, *ApJ*, **892**, 49  
 Hunter, J. D. 2007, *Comput. Sci. Eng.*, **9**, 90  
 Jaeggli, S. A., Lin, H., & Uitenbroek, H. 2012, *ApJ*, **745**, 133  
 Jess, D. B., Mathioudakis, M., Christian, D. J., et al. 2010, *Sol. Phys.*, **261**, 363  
 Jess, D. B., Morton, R. J., Verth, G., et al. 2015, *Space Sci. Rev.*, **190**, 103

- Judge, P. G., Tritschler, A., Uitenbroek, H., et al. 2010, *ApJ*, **710**, 1486
- Kilpua, E., Koskinen, H. E. J., & Pulkkinen, T. I. 2017, *Liv. Rev. Sol. Phys.*, **14**, 5
- Kobayashi, K., Cirtain, J., Winebarger, A. R., et al. 2014, *Sol. Phys.*, **289**, 4393
- Kowalski, A. F., Cauzzi, G., & Fletcher, L. 2015, *ApJ*, **798**, 107
- Lemen, J. R., Title, A. M., Akin, D. J., et al. 2012, *Sol. Phys.*, **275**, 17
- Lipartito, I., Judge, P. G., Reardon, K., & Cauzzi, G. 2014, *ApJ*, **785**, 109
- Löfdahl, M. 2012, *IAU Special Session*, **6**, E3.05
- Löfdahl, M. 2016, in *ASP Conf. Ser.*, **504**, Coimbra Solar Physics Meeting: Ground-based Solar Observations in the Space Instrumentation Era, eds. I. Dorotovic, C. E. Fischer, & M. Temmer, 111
- Löfdahl, M. G., Hillberg, T., de la Cruz Rodríguez, J., et al. 2021, *A&A*, **653**, A68
- Martínez Pillet V., Del Toro Iniesta, J. C., Álvarez-Herrero, A., et al. 2011, *Sol. Phys.*, **268**, 57
- Molnar, M. E., Reardon, K. P., Chai, Y., et al. 2019, *ApJ*, **881**, 99
- Murabito, M., Romano, P., Guglielmino, S. L., Zuccarello, F., & Solanki, S. K. 2016, *ApJ*, **825**, 75
- Murabito, M., Romano, P., Guglielmino, S. L., & Zuccarello, F. 2017, *ApJ*, **834**, 76
- Murabito, M., Ermolli, I., Giorgi, F., et al. 2019, *ApJ*, **873**, 126
- Murabito, M., Guglielmino, S. L., Ermolli, I., Stangalini, M., & Giorgi, F. 2020a, *ApJ*, **890**, 96
- Murabito, M., Shetye, J., Stangalini, M., et al. 2020b, *A&A*, **639**, A59
- Narukage, N., McKenzie, D. E., Ishikawa, R., et al. 2016, *SPIE Conf. Ser.*, **9905**, 990508
- Padoan, P., & Nordlund, Å. 2011, *ApJ*, **730**, 40
- Rast, M. P., Bello González, N., Bellot Rubio, L., et al. 2021, *Sol. Phys.*, **296**, 70
- Reardon, K. P., & Cavallini, F. 2008, *A&A*, **481**, 897
- Reardon, K. P., Uitenbroek, H., & Cauzzi, G. 2009, *A&A*, **500**, 1239
- Rempel, M., & Schlichenmaier, R. 2011, *Liv. Rev. Sol. Phys.*, **8**, 3
- Righini, A., Cavallini, F., & Reardon, K. P. 2010, *A&A*, **515**, A85
- Rimmele, T. R., Warner, M., Keil, S. L., et al. 2020, *Sol. Phys.*, **295**, 172
- Romano, P., Berrilli, F., Criscuoli, S., et al. 2012, *Sol. Phys.*, **280**, 407
- Romano, P., Frasca, D., Guglielmino, S. L., et al. 2013, *ApJ*, **771**, L3
- Romano, P., Zuccarello, F. P., Guglielmino, S. L., & Zuccarello, F. 2014, *ApJ*, **794**, 118
- Romano, P., Falco, M., Guglielmino, S. L., & Murabito, M. 2017, *ApJ*, **837**, 173
- Romano, P., Murabito, M., Guglielmino, S. L., Zuccarello, F., & Falco, M. 2020, *ApJ*, **899**, 129
- Romano, P., Guglielmino, S. L., Costa, P., et al. 2022, *Sol. Phys.*, **297**, 7
- Ruiz Cobo, B., Quintero Noda, C., Gafeira, R., et al. 2022, *A&A*, **660**, A37
- Scharmer, G. B., Bjelksjo, K., Korhonen, T. K., Lindberg, B., & Petterson, B. 2003, *SPIE Conf. Ser.*, **4853**, 341
- Scharmer, G. B., Narayan, G., Hillberg, T., et al. 2008, *ApJ*, **689**, L69
- Scharmer, G. B., Löfdahl, M. G., Sliepen, G., & de la Cruz Rodríguez, J. 2019, *A&A*, **626**, A55
- Scherrer, P. H., Bogart, R. S., Bush, R. I., et al. 1995, *Sol. Phys.*, **162**, 129
- Scherrer, P. H., Schou, J., Bush, R. I., et al. 2012, *Sol. Phys.*, **275**, 207
- Schilliro, F., & Romano, P. 2021, *MNRAS*, **503**, 2676
- Schlichenmaier, R., & Schmidt, W. 2000, *A&A*, **358**, 1122
- Schlichenmaier, R., Bellot Rubio, L. R., Collados, M., et al. 2019, ArXiv e-prints, [arXiv:1912.08650]
- Schmelz, J. T. 2003, *Advances in Space Research*, **32**, 895
- Seykora, E. J. 1993, *Sol. Phys.*, **145**, 389
- Sobotka, M., Del Moro, D., Jurčák, J., & Berrilli, F. 2012, *A&A*, **537**, A85
- Sobotka, M., Švanda, M., Jurčák, J., et al. 2013, *A&A*, **560**, A84
- Sobotka, M., Heinzel, P., Švanda, M., et al. 2016, *ApJ*, **826**, 49
- Solanki, S. K., & Montavon, C. A. P. 1993, *A&A*, **275**, 283
- Stangalini, M., Del Moro, D., Berrilli, F., & Jefferies, S. M. 2011, *A&A*, **534**, A65
- Stangalini, M., Giannattasio, F., Del Moro, D., & Berrilli, F. 2012, *A&A*, **539**, L4
- Stangalini, M., Berrilli, F., & Consolini, G. 2013, *A&A*, **559**, A88
- Stangalini, M., Jafarzadeh, S., Ermolli, I., et al. 2018, *ApJ*, **869**, 110
- Stangalini, M., Baker, D., Valori, G., et al. 2021a, *Philos. Trans. R. Soc. Lond. A*, **379**, 20200216
- Stangalini, M., Erdélyi, R., Boockock, C., et al. 2021b, *Nat. Astron.*, **5**, 691
- Stangalini, M., Jess, D. B., Verth, G., et al. 2021c, *A&A*, **649**, A169
- Stangalini, M., Verth, G., Fedun, V., et al. 2022, *Nat. Astron.*, **13**, 479
- Stein, R. F. 2012, *Liv. Rev. Sol. Phys.*, **9**, 4
- Straus, T., Fleck, B., Jefferies, S. M., et al. 2008, *ApJ*, **681**, L125
- Temmer, M. 2021, *Liv. Rev. Sol. Phys.*, **18**, 4
- Tritschler, A., Uitenbroek, H., & Reardon, K. 2008, *ApJ*, **686**, L45
- Tsuneta, S., Ichimoto, K., Katsukawa, Y., et al. 2008, *Sol. Phys.*, **249**, 167
- van Driel-Gesztelyi, L., & Green, L. M. 2015, *Liv. Rev. Sol. Phys.*, **12**, 1
- van Noort M., Rouppe van der Voort, L., & Löfdahl, M. G. 2005, *Sol. Phys.*, **228**, 191
- Vecchio, A., Cauzzi, G., Reardon, K. P., Janssen, K., & Rimmele, T. 2007, *A&A*, **461**, L1
- Vecchio, A., Cauzzi, G., & Reardon, K. P. 2009, *A&A*, **494**, 269
- Viavattene, G., Consolini, G., Giovannelli, L., et al. 2020, *Entropy*, **22**, 716
- Viavattene, G., Murabito, M., Guglielmino, S. L., et al. 2021, *Entropy*, **23**, 413
- Virtanen, P., Gommers, R., Oliphant, T. E., et al. 2020, *Nat. Methods*, **17**, 261
- Vissers, G., & Rouppe van der Voort, L. 2012, *ApJ*, **750**, 22
- Viticchié, B., Del Moro, D., Berrilli, F., Bellot Rubio, L., & Tritschler, A. 2009, *ApJ*, **700**, L145
- Viticchié, B., Del Moro, D., Criscuoli, S., & Berrilli, F. 2010, *ApJ*, **723**, 787
- Vourlidas, A., Beltran, S. T., Chintzoglou, G., et al. 2016, *J. Astron. Instrum.*, **5**, 1640003
- Wedemeyer, S., Szydlarski, M., Jafarzadeh, S., et al. 2020, *A&A*, **635**, A71
- Wiegelmann, T., & Sakurai, T. 2021, *Liv. Rev. Sol. Phys.*, **18**, 1
- Zuccarello, F., Romano, P., Guglielmino, S. L., et al. 2009, *A&A*, **500**, L5

## Appendix A: Data summary and metadata information

Table A.1 summarizes the information on the Level 1 data available in IBIS-A. These data consist of the observations processed for instrumental calibrations and restored for residual image degradation by seeing using the MOMFBD method. Table A.2 summarizes information on the Level 2 data available in IBIS-A. These data consist of the observations processed for data inversion using the VFISV code. More details on the Level 1 and Level 2 data can be found in Sect. 2.3.

Figures A.1 and A.2 show examples of metadata information provided in the keywords of the primary and extended headers of FITS files of the Level 0 data available in IBIS-A. Figure A.3 gives an example of the fields with information stored in the variable *info\_nb* relevant to Level 1 data. Figures A.4 and A.5 show examples of the metadata information provided in the keywords of the primary and extended headers of FITS files of the Level 1.5 data, respectively. Figure A.6 displays the same information for Level 2 data. See Sect. 3.1 for more details.

**Table A.1.** Overview of the Level 1 data available in IBIS-A.

Date YY-MM-DD	Time [UT]	Target <sup>(a)</sup>	Lambda <sup>(b)</sup> Points <sup>(c)</sup>	Scans
2008-10-15	16:30:00	PO	6173 IQUV (21), 8542 I (21)	80
2012-04-17	13:58:43	PO	6302 IQUV (30), 6173 IQUV (24) 8542 I (25)	56
	15:09:06	PO	6302 IQUV (30), 6173 IQUV (24) 8542 I (25)	68
	18:13:40	PO	6302 IQUV (30), 6173 IQUV (24) 8542 I (25)	100
2013-02-05	18:18:21	SP	6173 IQUV (5), 6563 I (14), 8542 IQUV (25)	61
2013-10-07	17:39:08	SP	6173 IQUV (10), 5896 IQUV (23)	137
2013-10-20	15:14:22	SP	6173 IQUV (10), 7090 I (10), 8542 IQUV (11)	175
	17:37:20	QS	5896 IQUV (10)	157
	18:11:51	QS	5896 IQUV (10)	137
2014-04-15	14:41:21	PO	6173 IQUV (5), 8542 I (11)	300
2014-04-21	14:15:33	PO	6173 IQUV (10x6), 8542 IQUV (11x6)	15
	15:17:03	PO	6173 IQUV (10x6), 8542 IQUV (11x6),	15
2014-10-14	15:15:57	PO	6173 IQUV (20), 6563 I (25), 8542 IQUV (25)	238
2014-10-22	14:29:34	SP	6173 IQUV (20), 6563 I (25), 8542 IQUV (25)	84
	15:46:24	SP	6173 IQUV (20), 6563 I (25), 8542 IQUV (25)	17
	16:05:36	SP	6173 IQUV (20), 6563 I (25), 8542 IQUV (25)	37
	17:43:40	PO	6173 IQUV (20), 6563 I (25), 8542 IQUV (25)	31
2015-04-10	14:34:25	SP	6173 IQUV (10), 8542 IQUV (11),	237
2015-04-11	14:14:40	PO	6173 IQUV (10x6), 8542 IQUV (11x6)	19
	15:01:55	PO	6173 IQUV (10x6), 8542 IQUV (11x6)	18
2015-04-30	13:52:44	QS	6173 IQUV (21), 8542 I (21)	290
2015-05-01	14:17:52	QS	6173 IQUV (21), 8542 IQUV (21)	58
2015-05-02	14:25:34	QS	6173 IQUV (21), 8542 IQUV (21)	50
	15:08:33	QS	6173 IQUV (21), 8542 IQUV (21)	20
	15:27:31	QS	6173 IQUV (21), 8542 IQUV (21)	79
2015-05-03	14:28:42	SP	6173 IQUV (21), 8542 IQUV (21)	85
	17:15:05	SP	6173 IQUV (21), 8542 IQUV (21)	25
2015-05-18	16:38:19	SP	6173 IQUV (24), 6302 IQUV (30), 8542 I (25), 6563 I (17)	20
2016-05-13	13:38:48	SP	6173 IQUV (21), 8542 IQUV (21)	50
	14:15:09	SP	6173 IQUV (21), 8542 IQUV (21)	58
	15:00:27	PO	6173 IQUV (21), 8542 IQUV (21)	163
2016-05-19	13:37:43	SP	6173 IQUV (21), 8542 IQUV (21)	100
2016-05-20	13:53:06	SP	6173 IQUV (21), 8542 IQUV (21)	319
2016-10-05	15:06:58	PO	8542 IQUV (11), 6563 I (14)	200
2016-10-06	15:58:20	QS	8542 IQUV (11), 6563 I (14)	200
	16:55:16	QS	8542 IQUV (11), 6563 I (14)	176
2016-10-10	17:12:08	PO	8542 IQUV (11), 6563 I (14)	200
	18:07:47	PO	8542 IQUV (11), 6563 I (14)	100
2016-10-11	16:04:17	QS	6173 IQUV (20), 8542 IQUV (25), 6563 I (14)	29

Table A.1. continued.

Date YY-MM-DD	Time [UT]	Target <sup>(a)</sup>	Lambda <sup>(b)</sup> Points <sup>(c)</sup>	Scans
2016-10-12	16:33:07	QS	6173 IQUV (20), 8542 IQUV (25), 6563 I (14)	31
	14:53:30	QS	6173 IQUV (20), 8542 IQUV (25), 6563 I (14)	100
	16:31:47	SP	8542 IQUV (11), 6563 I (14)	5
	16:38:46	SP	8542 IQUV (11), 6563 I (14)	200
2016-10-14	17:32:08	SP	8542 IQUV (11), 6563 I (14)	85
	14:53:57	QS	6173 IQUV (20), 5896 IQUV (10), 6563 I (14)	150
	16:25:24	SP	8542 IQUV (11), 6563 I (14)	228
2016-10-17	15:24:24	QS	6173 IQUV (20), 8542 IQUV (25), 6563 I (14)	74
2016-10-18	15:12:40	QS	6173 IQUV (20), 8542 IQUV (25), 6563 I (14)	58
2016-10-21	16:00:14	QS	6173 IQUV (20), 8542 IQUV (25), 6563 I (14)	60
	17:00:34	PO	8542 IQUV (11), 6563 I (14)	232
2017-05-05	14:06:00	PO	6173 IQUV (21), 8542 IQUV (21)	85
	15:37:49	QS	6173 IQUV (21), 8542 IQUV (21)	107
2017-05-12	13:34:16	QS	6173 IQUV (21), 8542 IQUV (21)	40
2017-11-10	15:12:46	QS	8542 I (30), 5896 I (19)	347
2018-02-01	17:06:03	QS	8542 I (30), 5896 I (19)	149
	17:44:02	QS	8542 I (30), 5896 I (19)	147
2018-04-11	16:05:05	QS	8542 I (30), 5896 I (19)	293
2018-04-26	15:48:38	PO	8542 I (27), 5896 I (24)	199
2018-05-18	14:01:10	PO	8542 I (30), 6563 I (17), 5896 I (19)	365
2018-05-19	14:01:17	PO	8542 I (29), 6563 I (27), 5896 I (19)	215
2018-06-20	13:53:05	SP	8542 I (29), 6563 I (27), 5896 I (19)	185
2018-06-21	13:57:00	QS	8542 I (29), 6563 I (27)	315
	15:22:32	QS	8542 I (29), 6563 I (27)	10
	15:53:12	QS	8542 I (29), 6563 I (27)	10
	16:21:09	QS	8542 I (29), 6563 I (27)	10
	16:32:05	QS	8542 I (29), 6563 I (27)	10
	14:29:32	QS	8542 I (29), 6563 I (27)	182
	15:18:55	QS	8542 I (29), 6563 I (27)	253
2018-06-25	14:31:04	QS	8542 I (30), 6563 I (27)	190
	15:22:10	QS	8542 I (30), 6563 I (27)	182
	16:13:17	QS	8542 I (30), 6563 I (27)	127
2018-06-26	13:35:58	QS	8542 I (30), 6563 I (27)	179
	14:25:00	QS	8542 I (30), 6563 I (27)	180
	15:13:44	QS	8542 I (30), 6563 I (27)	177
	16:02:50	QS	8542 I (30), 6563 I (27)	130
2018-06-27	13:40:50	QS	8542 I (30), 6563 I (27)	213
	14:41:01	QS	8542 I (30), 6563 I (27)	190
	15:36:14	QS	8542 I (30), 6563 I (27)	213
	16:51:11	QS	8542 I (30), 6563 I (27)	5
	16:54:46	QS	8542 I (30), 6563 I (27)	5
	17:10:40	QS	8542 I (30), 6563 I (27)	5
	17:14:48	QS	8542 I (30), 6563 I (27)	5
2018-07-05	14:11:11	QS	8542 I (30), 6563 I (27)	68
	14:35:16	QS	8542 I (30), 6563 I (27)	5
	14:41:09	QS	8542 I (30), 6563 I (27)	5
	14:46:33	QS	8542 I (30), 6563 I (27)	5
	14:54:33	QS	8542 I (30), 6563 I (27)	5
2018-06-16	13:53:21	QS	8542 I (30), 6563 I (27)	106
	14:50:04	QS	8542 I (30), 6563 I (27)	106
2018-07-17	13:33:46	QS	8542 I (30), 6563 I (27)	122
	14:28:21	QS	8542 I (30), 6563 I (27)	116
2018-07-23	14:02:33	QS	8542 I (30), 6563 I (27)	3
	14:03:41	QS	8542 I (30), 6563 I (27)	139
2018-08-16	14:41:02	QS	8542 I (30), 6563 I (27)	151
	14:15:34	QS	8542 I (30)	573
	14:01:21	QS	8542 I (30)	582
2018-09-24	14:34:27	QS	8542 I (30), 6563 I (27)	201
	15:33:56	QS	8542 I (30), 6563 I (27)	141
2018-09-25	14:09:52	QS	8542 I (30), 6563 I (27)	196

Table A.1. continued.

Date YY-MM-DD	Time [UT]	Target <sup>(a)</sup>	Lambda <sup>(b)</sup> Points <sup>(c)</sup>	Scans
	15:32:27	QS	8542 I (30), 6563 I (27)	145
2018-10-04	20:29:11	QS	8542 I (30), 6563 I (27)	22
2018-10-10	15:06:09	QS	8542 I (30), 6563 I (27)	146
2018-11-02	15:11:37	QS L	8542 I (25)	900
	16:28:55	QS L	8542 I (25)	509
2018-11-03	15:35:59	QS L	8542 I (25)	900
	16:45:31	QS L	8542 I (25)	900
	17:54:54	QS L	8542 I (25)	900
2018-11-04	15:00:54	QS L	8542 I (25)	619
	15:54:45	QS L	8542 I (25)	900
	17:04:22	QS L	8542 I (25)	900
	18:13:46	QS L	8542 I (25)	175
	18:38:28	QS L	8542 I (25)	99
2018-11-15	15:16:49	PO	8542 I (30), 6563 I (27)	316
	17:20:28	QS	8542 I (30), 6563 I (27)	190
	15:05:40	PO	8542 I (30), 6563 I (27)	31
2018-11-16	15:13:26	PO	8542 I (30), 6563 I (27)	189
	16:10:14	QS	8542 I (30), 6563 I (27)	188
2018-11-19	15:33:04	PO	8542 I (30), 6563 I (27)	163
	16:09:27	PO	8542 I (30), 6563 I (27)	266
2018-11-27	16:58:08	QS	8542 I (30), 6563 I (27)	244
2018-11-29	15:35:31	QS	8542 I (30), 6563 I (27)	126
2018-12-04	16:28:59	QS	8542 I (30), 6563 I (27)	279
2018-12-20	15:55:00	QS L	8542 I (21), 6563 I (23)	15
	16:04:54	QS	8542 I (21), 6563 I (23)	10
	17:25:17	QS	8542 I (21), 6563 I (23)	100
2018-12-23	15:15:32	QS	8542 I (21), 6563 I (23)	120
	17:19:24	QS	8542 I (21), 6563 I (23)	120
	17:53:06	QS	8542 I (21), 6563 I (23)	120
	18:25:34	QS	8542 I (21), 6563 I (23)	120
2019-01-25	15:40:56	PO	8542 I (30), 6563 I (27), 5896 I (19)	25
	15:52:35	PO	8542 I (30), 6563 I (27), 5896 I (19)	160
	17:27:47	PO	8542 I (30), 6563 I (27), 5896 I (19)	48
	17:46:32	PO	8542 I (30), 6563 I (27), 5896 I (19)	55
2019-02-18	15:39:03	QS	8542 I (30), 6563 I (27)	127
2019-02-25	14:52:08	QS L	8542 I (30), 6563 I (27)	130
	15:25:23	QS L	8542 I (30), 6563 I (27)	146

**Notes.** <sup>(a)</sup> Target: PO: pore, SP: sunspot, QS: quiet sun, QS L: Quiet Sun Limb. <sup>(b)</sup> Lambda: Spectral lines observed with IBIS. <sup>(c)</sup> Points describes the number of spectral positions sampled in the line. Observing modes with multiple exposures at each point are reported as  $n \times m$ , where  $n$  and  $m$  are the number of spectral points and the number of exposures at each point, respectively.



**Level 0: Primary Header**

```

SIMPLE = T / FITS STANDARD
BITPIX = 16 / 16 BITS:INTEGER*2; 8 BITS:INTEGER*1
NAXIS = 0 / NUMBER OF AXES
EXTEND = T / True = EXTENSIONS MAY BE PRESENT IN FILE
BINNING = 1 / BINNING FACTOR
BSCALE = 1.0000E+00 / TRUE=(FITS VALUE)*BSCALE + BZERO
BZERO = 0.000 / THE OFFSET
BUNIT = 'Counts' / PIXEL VALUE
DATE = '2012-05-28T13:38:43.687' / DATE THE FILE WAS WRITTEN yyyy-mm-dd
ORIGIN = 'NSO/SP' / DST
TELESCOP = 'NSO - DST' / NAME OF THE TELESCOPE
INSTRUME = 'IBIS' / INSTRUMENT USED TO ACQUIRE THE DATA
DETECTOR = 'ANDOR iXon 885' / DETECTOR USED TO ACQUIRE THE DATA
FILENAME = 'ScienceObservation\20120528_133837\s000.ScienceObservation.fits' / DA
FILEORIG='ScienceObservation\20120528_133837\s000.ScienceObservation.fits' / OR
DATE-OBS = '2012-05-28T13:38:43.676' / STARTING DATE AND TIME IN U.T.
DATE-END = '2012-05-28T13:38:43.736' / ENDING DATE AND TIME IN U.T.
CCD_TEMP = -60 / CCD SENSOR TEMP
EXP_EFF = 0.0600 / ACTUAL EXPOSURE TIME SEC
GAIN_PRE = 'X2' / PRE-AMPLIFIER GAIN
GAIN_EM = 0 / ELECTRON MULTIPLIER GAIN
SER_NUM = 2748 / CAMERA SERIAL NUMBER
OBSERVER = 'Mike/Doug' / TELESCOPE OPERATORS
WL_PRFLT = '620' / WHITE LIGHT CAMERA PRE-FILTER WAVELENGTH
CHANNEL = 'Narrowband' / CAMERA IDENTIFER
SEQ_NUM = 's000' / SEQUENCE NUMBER (sxxx)
SERIESID = '20120528_133837' / SAME TEXT AS PARENT DIRECTORY
BASECLMP = 100 / Baseline clamp value
X_START = 1 / X Start position of image
Y_START = 1 / Y Start position of image
END

```

**Fig. A.1.** Example of metadata information stored in the FITS primary header of the Level 0 data available in IBIS-A for the observations taken on 28 May 2012 at 13:38:43 UT.

**Level 0: Extended Header**

```

XTENSION = 'IMAGE' / FITS EXTENDED
BITPIX = 16 / 16 BITS:INTEGER*2; 8 BITS:INTEGER*1
NAXIS = 2 / NUMBER OF AXES
NAXIS1 = 1000 / NUMBER OF ELEMENTS ALONG AXIS1
NAXIS2 = 1000 / NUMBER OF ELEMENTS ALONG AXIS2
PCOUNT = 0 / required keyword; must = 0
GCOUNT = 1 / required keyword; must = 1
NIMAGES = 349 / EXPECTED NUMBER OF IMAGES PER FITS FILE
BZERO = 0.000 / THE OFFSET
BSCALE = 1.0 / DEFAULT SCALING FACTOR
EXPTIME = 0.060 / EXPOSURE TIME IN SECONDS
DATE-OBS = '2012-05-28T13:38:43.689' / STARTING DATE AND TIME IN U.T.
DATE-END = '2012-05-28T13:38:43.749' / ENDING DATE AND TIME IN U.T.
FILTER = 1 / COMMANDED POSITION OF THE FILTER WHEEL
WAVELNTH = +6302.1802 / THE (APPROXIMATE ABS) WAVELENGTH OF THE OBSERVA
REL_WAVE = +0.2335 / WAVELENGTH RELATIVE TO IBIS FILTER CENTER
WAVEUNIT = -10 / WAVELENGTH UNITS USED IN THE OBSERVATION 10^(WAVEUNIT) m
FP1_VOLT = -122.0 / VOLTAGE SETTING TO CS100 CONTROLLER OF FP1
FP2_VOLT = -67.0 / VOLTAGE SETTING TO CS100 CONTROLLER OF FP2
LCVR1_RE = 360.0 / COMMANDED RETARDANCE TO LCVR #1
LCVR2_RE = 360.0 / COMMANDED RETARDANCE TO LCVR #2
LCVR1_V = 2.067 / VOLTAGE SETTING TO LCVR #1
LCVR2_V = 2.097 / VOLTAGE SETTING TO LCVR #2
STOKES = 'I+Q' / STOKES PARAMETER
BUF_INFO = 0 / Number of CamImg in ring buffer
FRAMENUM = 0 / Image Number in this series (ZERO based)
DST_TIME = '2012-05-28T13:38:34.712' / When DST info was last updated (UTC)
DST_AZ = 7.603146100000E+01 / DST turret azimuth (degrees)
DST_EL = 1.896153400000E+01 / DST turret elevation (degrees)
DST_TBL = 3.526300200000E+02 / DST table position (degrees)
DST_GDRN = 1.327530400000E+01 / DST guider angle (degrees)
DST_XGDR = -1.709163300000E+02 / DST guider X-axis position (arcsec)
DST_YGDR = -1.946493400000E+02 / DST guider Y-axis position (arcsec)
DST_SLAT = -1.385126800000E+01 / Stonyhurst Heliographic solar lat. (deg)
DST_SLNG = -9.360190900000E+00 / Stonyhurst Heliographic solar long. (deg)
DST_HPA = 1.445608000000E+02 / Heliocentric position angle (degrees)
DST_GPA = 1.280135200000E+02 / Geocentric position angle (degrees)
DST_RV = 2.735441300000E-01 / Heliocentric radius vector
DST_PEE = -1.654727800000E+01 / Solar P angle (degrees)
DST_BEE0 = -1.045614200000E+00 / Solar B0 angle (degrees)
DST_ELL0 = -5.105618400000E+01 / Solar L0 angle (degrees)
DST_SDIM = 1.893940400000E+03 / Solar diameter (arcsec)
DST_LLVL = 4.165039100000E+00 / DST guider light level
DST_SEE = 1.367187500000E-01 / Seykora scintillation monitor value (arcsec)
DST_SAZ = 7.601885400000E+01 / Solar azimuth (degrees)
DST_SEL = 1.903249500000E+01 / Solar elevation (degrees)
PT4_TIME = '2012-05-28T13:22:06.933' / When PT4 info was last updated (UTC)
PT4_PSTG = 'OUT' / Port 4 cal unit polarizer stage position
PT4_POL = 4.400000000000E-02 / Port 4 cal unit polarizer position (degrees)
PT4_RSTG = 'OUT' / Port 4 cal unit retarder stage position
PT4_RET = 4.400000000000E-02 / Port 4 cal unit retarder position (degrees)
PT4_MIR = 'OUT' / Port 4 lamp mirror position
PT4_FS = 'USER1' / Port 4 field stop position
SEQ_CTR = 0 / IMAGE NUMBER WITHIN EACH SEQ (ZERO based)
END

```

**Fig. A.2.** Example of metadata information stored in the FITS extended header of the Level 0 data available in IBIS-A for the observations taken on 28 May 2012 at 13:38:43 UT.

**Level 1: info\_nb variable**

```

** Structure <2557978>, 37 tags, length=7712, data length=7700, refs=1:
FILENAME      STRING      Array[126]
EXTENSION     LONG        Array[126]
TIME          DOUBLE     Array[126]
FILTER        LONG        Array[126]
EXPTIME       DOUBLE     Array[126]
WAVE          DOUBLE     Array[126]
GRID          DOUBLE     Array[126]
FPI1          FLOAT      Array[126]
FPI2          FLOAT      Array[126]
LCVR1         FLOAT      Array[126]
LCVR2         FLOAT      Array[126]
STOKES        STRING     Array[126]
FRAME         DOUBLE     Array[126]
DST_TIME      DOUBLE     Array[126]
DST_AZ        DOUBLE     Array[126]
DST_EL        DOUBLE     Array[126]
DST_TBL       FLOAT      Array[126]
DST_GDRN      DOUBLE     Array[126]
DST_XGDR      DOUBLE     Array[126]
DST_YGDR      DOUBLE     Array[126]
DST_SLAT      DOUBLE     Array[126]
DST_SLNG      DOUBLE     Array[126]
DST_RV        DOUBLE     Array[126]
DST_PEE       DOUBLE     Array[126]
DST_BEE       DOUBLE     Array[126]
DST_ELL       DOUBLE     Array[126]
DST_SDIM      DOUBLE     Array[126]
DST_LLEVEL    DOUBLE     Array[126]
DST_SEE       DOUBLE     Array[126]
DST_SAZ       DOUBLE     Array[126]
DST_SEL       DOUBLE     Array[126]
PT4_TIME      DOUBLE     Array[126]
PT4_PSTG      STRING     Array[126]

```

**Fig. A.3.** Example of several fields with information stored in the *info\_nb* variable, which is relevant to the Level 1 data derived from the spectropolarimetric observations taken at the Fe I 617.3 nm line on 13 May 2016 at 13:38:48 UT.

**Level 1.5: Primary Header**

```

SIMPLE = T / Written by IDL: Mon Nov 15 12:29:57 2021
BITPIX = 8 /
NAXIS = 0 /
DATE = 'Mon Jan 31 11:07:25 2022' / Date of FITS file creation
EXTEND = T / FILE MAY CONTAIN EXTENSIONS
EXTNAME = 'science' / Science-ready Level 1.5
SOLARNET = 0.500000 / Fully SOLARNET-compliant=1.0, partially=0.5
OBS_HDU = 1 / This HDU contains observational data
BTYYPE = 'Output' / Physical quantities / CP, LP, NCP and Vel field
DATE-BEG = '2016-05-13T13:38:48' / STARTING DATE AND TIME IN U.T.
OBSRVTRY = 'NSO, Sacramento Peak' / Name of observatory
TELESCOP = 'DST' / Name of the telescope
INSTRUME = 'IBIS' / Name of instrument
OBS_MODE = 'Spectropolarimetric imaging' / settings used during obs.
WAVEBAND = 'Fe I 6173 A - Ca II 8542 A' / PRE-FILTER names
SCAN_DUR = 19.973000 / Time require for line scan
DST_SLAT = 11.586998 / Stonyhurst Heliographic solar lat. (deg)
DST_SLNG = 45.541883 / Stonyhurst Heliographic solar long. (deg)
SOLAR P0 = -21.240328 / Solar P angle (degrees)
SOLAR B0 = -2.7994148 / Solar B0 angle (degrees)
SOLAR L0 = -1.1516182 / Solar L0 angle (degrees)
RSUN_ARC = 949.71210 / Apparent photospheric Solar radius in arc second
DST_SEE = 0.31494141 / Mean Seykora scintillation monitor value arcsec
PRSTEP1 = 'CALIBRATION' / Bias, dark and flatfielding correction
PRPROC1 = 'INAF IBIS pipeline' / Name of procedure used written in IDL
PRSTEP2 = 'SPECTRAL-DISTORTION-CORRECTION' / Blueshift and gain correction
PRPROC2 = 'INAF IBIS pipeline' / Name of procedure used written in IDL
PRSTEP3 = 'DESTRETCHING' / MOMFBD output
PRPROC3 = 'INAF IBIS pipeline' / Name of procedure used written in IDL
PRSTEP4 = 'DEMODULATION' /
PRPROC4 = 'INAF IBIS pipeline' / Name of procedure used written in IDL
PRSTEP5 = 'STOKES-CROSSTALK-CORRECTION' /
PRPROC5 = 'INAF IBIS pipeline' / Name of procedure used written in IDL
PRSTEP6 = 'PHYSICAL QUANTITIES COMPUTATION' / Processing step
ORIGIN = 'INAF - OAR' / Creator of FITS files
LEVEL = '1.5' / Data level of FITS file
INFO_URL = 'http://ibis.oa-roma.inaf.it/IBISA/' / IBIS archive web page
END

```

**Fig. A.4.** Example of metadata information stored in the FITS primary header of the Level 1.5 data available in IBIS-A for the observations taken on 13 May 2016 at 13:38:48 UT.

**Level 1.5: ext=1 Header**

```

XTENSION = 'IMAGE' / IMAGE extension
BITPIX = -32 /
NAXIS = 3 /
NAXIS1 = 350 /
NAXIS2 = 800 /
NAXIS3 = 10 /
PCOUNT = 0 / NO GROUP PARAMETERS
GCOUNT = 1 / ONE TABLE
POS 0 = 'Cont' / Continuum intensity
POS 1 = 'CP1_6173' / CP1 / Circular polarization for Fe I 6173 A
POS 2 = 'CP2_6173' / CP2 / Circular polarization for Fe I 6173 A
POS 3 = 'LP_6173 ' / LP / Linear polarization for Fe I 6173 A
POS 4 = 'NCP_6173' / NCP / Net Circular polarization for Fe I 6173 A
POS 5 = 'CP1_8542' / CP1 / Circular polarization for Ca II 8542 A
POS 6 = 'CP2_8542' / CP2 / Circular polarization for Ca II 8542 A
POS 7 = 'LP_8542 ' / LP / Linear polarization for Ca II 8542 A
POS 8 = 'NCP_8542' / NCP / Net Circular polarization for Ca II 8542 A
POS 9 = 'Vlos_6173' / Vlos / Fe I Line-of-sight Velocity field (km/s)
END

```

**Level 1.5: ext=2 Header**

```

XTENSION = 'wavelength values' / IMAGE extension
BITPIX = -32 /
NAXIS = 2 /
NAXIS1 = 2 /
NAXIS2 = 21 /
PCOUNT = 0 / NO GROUP PARAMETERS
GCOUNT = 1 / ONE TABLE
WAVE1 = 'Fe I 6173 A' /
NPOINTS1 = 21 / Number of spectral points for Fe I
WAVE2 = 'Ca II 8542 A' /
NPOINTS2 = 21 /Number of spectral points for Ca II
END

```

**Fig. A.5.** Example of metadata information stored in the FITS extended header of the Level 1.5 data available in IBIS-A for the observations taken on 13 May 2016 at 13:38:48 UT.

**Level 2: Primary Header**

```

SIMPLE = T / Written by IDL: Mon Nov 15 12:29:57 2021
BITPIX = 8 /
NAXIS = 0 /
DATE = 'Mon Nov 15 12:29:57 2021' / Date of FITS file creation
EXTEND = T / FILE MAY CONTAIN EXTENSIONS
EXTNAME = 'science ' / Name of HDU
SOLARNET = 0.500000 / Fully SOLARNET-compliant=1.0, partially=0.5
OBS_HDU = 1 / This HDU contains observational data
BTYPE = 'Output inversion' / Description of what the data array represents
DATE-BEG = '2016-05-13T13:38:48' / Date of start of observations
TIMESYS = 'UTC ' /
OBSRVTRY = 'NSO, Sacramento Peak' / Name of observatory
TELESCOP = 'DST ' / Name of the telescope
INSTRUME = 'IBIS ' / Name of instrument
OBS_MODE = 'Spectropolarimetric imaging' /s ettings used during obs.
PX_SCALE = '0.098" ' / Pixel scale of the image
WAVEBAND = 'Fe I 6173 A' / PRE-FILTER name
SCAN_DUR = 19.973000 / Time required for line scan
DST_SLAT = 11.586998 / Stonyhurst Heliographic solar lat. (deg)
DST_SLNG = 45.541883 / Stonyhurst Heliographic solar long. (deg)
SOLAR P0 = -21.240328 / Solar P angle (degrees)
SOLAR B0 = -2.7994148 / Solar B0 angle (degrees)
SOLAR L0 = -1.1516182 / Solar L0 angle (degrees)
RSUN_ARC = 949.71210 / Apparent photospheric Solar radius in arc second
DST_SEE = 0.31494141 / Mean Seykora scintillation monitor value arcsec
PRSTEP1 = 'CALIBRATION' / Bias, dark and flatfielding correction
PRPROC1 = 'INAF IBIS pipeline' / Name of procedure used written in IDL
PRSTEP2 = 'SPECTRAL-DISTORTION-CORRECTION' / Blueshift and gain correction
PRPROC2 = 'INAF IBIS pipeline' / Name of procedure used written in IDL
PRSTEP3 = 'DESTRETCHING' / MOMFBD output
PRPROC3 = 'INAF IBIS pipeline' / Name of procedure used written in IDL
PRSTEP4 = 'DEMODULATION' /
PRPROC4 = 'INAF IBIS pipeline' / Name of procedure used written in IDL
PRSTEP5 = 'STOKES-CROSSTALK-CORRECTION' /
PRPROC5 = 'INAF IBIS pipeline' / Name of procedure used written in IDL
PRSTEP6 = 'STOKES-INVERSION' / Processing step
PRPROC6 = 'VFISV ' / Name of procedure used
ORIGIN = 'INAF - OAR' / Creator of FITS files
LEVEL = '2 ' / Data level of FITS file
INFO_URL = 'http://ibis.oa-roma.inaf.it/IBISA/' / IBIS archive web page
END

```

**Level 2: ext=1 Header**

```

XTENSION = 'IMAGE ' / IMAGE extension
BITPIX = -32 /
NAXIS = 3 / Number of Axes
NAXIS1 = 350 / Spatial coordinates
NAXIS2 = 800 / Spatial coordinates
NAXIS3 = 6 / VFISV physical quantities
PCOUNT = 0 / NO GROUP PARAMETERS
GCOUNT = 1 / ONE TABLE
POS 0 = 'Cont' / Continuum intensity
POS 1 = 'B ' / VFISV /Magnetic field strength
POS 2 = 'Inc ' / VFISV /Inclination angle (degree)
POS 3 = 'Azi ' / VFISV /Azimuth angle (degree)
POS 4 = 'VLOS ' / VFISV /Line-of-sight Velocity field (km/s)
POS 5 = 'Ffact ' / VFISV /Filling factor
END

```

**Level 2: ext=2 Header**

```

XTENSION = 'wavelength values' / IMAGE extension
BITPIX = -32 /
NAXIS = 1 /
NAXIS1 = 21 /
PCOUNT = 0 / NO GROUP PARAMETERS
GCOUNT = 1 / ONE TABLE
N POINTS = 21 / Number of spectral points
END

```

**Fig. A.6.** Example of metadata information stored in the FITS header of the Level 2 data available in IBIS-A for the observations taken on 13 May 2016 at 13:38 UT.

**Table A.2.** Overview of the Level 2 data available in IBIS-A.

Date YY-MM-DD	Time [UT]	Target <sup>(a)</sup>	Data <sup>(b)</sup> from 6173 Å IUQV	Other data <sup>(c)</sup> available	Scans
2012-04-17	13:58:43	PO	B, B <sub>inc</sub> , B <sub>azi</sub> , F <sub>fact</sub> , V <sub>los</sub>	6302 IUQV, 8542 I	56
2012-04-17	15:09:06	PO	B, B <sub>inc</sub> , B <sub>azi</sub> , F <sub>fact</sub> , V <sub>los</sub>	6302 IUQV, 8542 I	68
2012-04-17	18:43:40	PO	B, B <sub>inc</sub> , B <sub>azi</sub> , F <sub>fact</sub> , V <sub>los</sub>	6302 IUQV, 8542 I	100
2013-10-07	17:39:08	SP	B, B <sub>inc</sub> , B <sub>azi</sub> , F <sub>fact</sub> , V <sub>los</sub>	5896 IUQV	130
2014-04-21	14:15:33	PO	B, B <sub>inc</sub> , B <sub>azi</sub> , F <sub>fact</sub> , V <sub>los</sub>	8542 IUQV	15
2014-10-14	15:15:57	PO	B, B <sub>inc</sub> , B <sub>azi</sub> , F <sub>fact</sub> , V <sub>los</sub>	8542 IUQV, 6563 I	238
2015-04-10	14:34:25	SP	B, B <sub>inc</sub> , B <sub>azi</sub> , F <sub>fact</sub> , V <sub>los</sub>	8542 IUQV	237
2015-04-11	14:14:40	PO	B, B <sub>inc</sub> , B <sub>azi</sub> , F <sub>fact</sub> , V <sub>los</sub>	8542 IUQV	19
2015-04-11	15:01:55	PO	B, B <sub>inc</sub> , B <sub>azi</sub> , F <sub>fact</sub> , V <sub>los</sub>	8542 IUQV	18
2015-04-30	13:52:44	QS	B, B <sub>inc</sub> , B <sub>azi</sub> , F <sub>fact</sub> , V <sub>los</sub>	8542 I	290
2015-05-01	14:17:52	QS	B, B <sub>inc</sub> , B <sub>azi</sub> , F <sub>fact</sub> , V <sub>los</sub>	8542 IUQV	58
2015-05-02	14:25:34	QS	B, B <sub>inc</sub> , B <sub>azi</sub> , F <sub>fact</sub> , V <sub>los</sub>	8542 IUQV	50
2015-05-02	15:08:33	QS	B, B <sub>inc</sub> , B <sub>azi</sub> , F <sub>fact</sub> , V <sub>los</sub>	8542 IUQV	20
2015-05-02	15:27:31	QS	B, B <sub>inc</sub> , B <sub>azi</sub> , F <sub>fact</sub> , V <sub>los</sub>	8542 IUQV	79
2015-05-03	14:28:42	SP	B, B <sub>inc</sub> , B <sub>azi</sub> , F <sub>fact</sub> , V <sub>los</sub>	8542 IUQV	85
2015-05-03	17:15:05	SP	B, B <sub>inc</sub> , B <sub>azi</sub> , F <sub>fact</sub> , V <sub>los</sub>	8542 IUQV	25
2016-05-13	13:38:48	SP	B, B <sub>inc</sub> , B <sub>azi</sub> , F <sub>fact</sub> , V <sub>los</sub>	8542 IUQV	50
2016-05-13	14:15:05	SP	B, B <sub>inc</sub> , B <sub>azi</sub> , F <sub>fact</sub> , V <sub>los</sub>	8542 IUQV	58
2016-05-13	15:00:27	PO	B, B <sub>inc</sub> , B <sub>azi</sub> , F <sub>fact</sub> , V <sub>los</sub>	8542 IUQV	163
2016-05-19	13:37:43	SP	B, B <sub>inc</sub> , B <sub>azi</sub> , F <sub>fact</sub> , V <sub>los</sub>	8542 IUQV	100
2016-05-20	13:53:06	SP	B, B <sub>inc</sub> , B <sub>azi</sub> , F <sub>fact</sub> , V <sub>los</sub>	8542 IUQV	319
2016-10-11	16:04:17	QS	B, B <sub>inc</sub> , B <sub>azi</sub> , F <sub>fact</sub> , V <sub>los</sub>	8542 IUQV, 6563 I	29
2016-10-11	16:33:07	QS	B, B <sub>inc</sub> , B <sub>azi</sub> , F <sub>fact</sub> , V <sub>los</sub>	8542 IUQV, 6563 I	31
2016-10-12	14:53:30	QS	B, B <sub>inc</sub> , B <sub>azi</sub> , F <sub>fact</sub> , V <sub>los</sub>	8542 IUQV, 6563 I	100
2017-05-05	14:06:00	PO	B, B <sub>inc</sub> , B <sub>azi</sub> , F <sub>fact</sub> , V <sub>los</sub>	8542 IUQV	85
2017-05-05	15:37:49	QS	B, B <sub>inc</sub> , B <sub>azi</sub> , F <sub>fact</sub> , V <sub>los</sub>	8542 IUQV	107
2017-05-12	13:34:16	QS	B, B <sub>inc</sub> , B <sub>azi</sub> , F <sub>fact</sub> , V <sub>los</sub>	8542 IUQV	40

**Notes.** <sup>(a)</sup> Target: PO: pore, SP: sunspot, QS: quiet sun, QS L: Quiet Sun Limb. <sup>(b)</sup> Data: Level 2 data from Fe I 6173 Å IUQV observations. B, B<sub>inc</sub>, B<sub>azi</sub>, and F<sub>fact</sub> refer to the magnetic field strength, inclination, azimuth, and filling factor, respectively. V<sub>los</sub> is the longitudinal component of the velocity field. <sup>(c)</sup> Other data available: Other spectral lines observed with IBIS. Line core is given in Å.